Wegener Center for Climate and Global Change
University of Graz
Leechgasse 25, A-8010 Graz, Austria

Atmospheric Remote Sensing and Climate System Research Group
EOPSCLIM Project Report

WegCenter/UniGraz Technical Report for FFG-ALR No. 1/2008

FFG-ALR study:
EOPSCLIM – End-to-end Occultation Processing System and Climate Monitoring Service
[Contract No: ALR-OEWP-CO-414/07]

EGOPS Enhancement Report

End-to-end Generic Occultation Performance Simulation and Processing System EGOPS: Enhancement of GPS RO Data Processing and IR Laser Occultation Capabilities

S. Schweitzer, B. Pirscher, M. Pock, F. Ladstädter, M. Borsche, U. Foelsche, J. Fritzer, and G. Kirchengast

Wegener Center for Climate and Global Change (WegCenter),
University of Graz, Graz, Austria

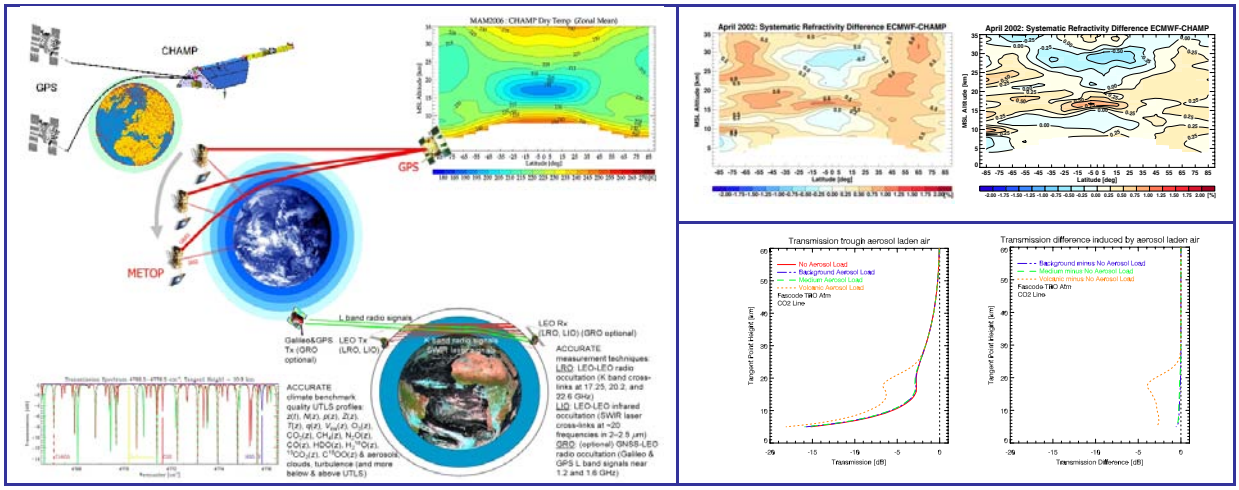

May 2008

(intentionally left blank; back page if double-sided print)

Table of Contents

(intentionally left blank; back page if double-sided print)

List of Acronyms

ACCURAID	Aid to ACCURATE Climate Satellite Mission Preparations (FFG-ALR project 2006-07)
ACCURATE	Atmospheric Climate and Chemistry in the UTLS Region and climate Trends Explorer
ALPS	ACCURATE LIO Performance Simulator
API	Application Program Interface
$C^{18}OO$	Carbon dioxide isotope (with one heavy-oxygen atom ^{18}O)
CCRv2.3	CHAMPCLIM Retrieval version 2.3
CDAAC	COSMIC Data Analysis and Archive Center (of UCAR, Boulder)
CHAMP	CHAllenging Minisatellite Payload for geoscientific research
CHAMPCLIM	Radio occultation data analysis advancement and climate change monitoring based on the CHAMP/GPS experiment (joint research project of the WegCenter and the GFZ Potsdam 2002-05)
COSMIC	Constellation Observing System for Meteorology, Ionosphere, and Climate
CO_2	Carbon dioxide
CPC	Climate Prediction Center
ECMWF	European Centre for Medium-Range Weather Forecasts (Reading, U.K.)
EGOPS5	End-to-end Generic Occultation Performance Simulator, Version 5
EGOPS6	End-to-end Generic Occultation Performance Simulation and Processing System
EOPSCLIM	End-to-end Occultation Processing System and Climate Monitoring Service (FFG-ALR study)
ERBS	Earth Radiation Budget Satellite
ESA	European Space Agency
ESA-Prodex	An ESA Programme line (for an enlisted subgroup of member states, incl. Austria)
EUMETSAT	European organisation for the exploitation of METeorological SATellites
FASCODE	FASt Atmospheric Signature CODE (here name for standard atmospheres)
FFG-ALR	Österr. Forschungsförderungsgesellschaft–Agentur für Luft- und Raumfahrt
FoMod	Forward Modeling System, subsystem of EGOPS
Formosat-3	FORMOsa SATellite 3 (same as COSMIC mission, Taiwanese original name)
FWF	Fonds zur Förderung der wissenschaftlichen Forschung (Austrian Science Fund)
Galileo	European future global navigation satellite system (part of GNSS)
GCM	Global Circulation Model
GEOS	Goddard Earth Observing System
GFZ	GeoForschungsZentrum Potsdam
GNSS	Global Navigation Satellite System (generic term, comprising the Global Positioning System GPS, Galileo, Glonass, Compass)
GPS	Global Positioning System
GPS/Met	GPS Meteorology – "proof of concept" experiment for the GPS RO technique
GRACE	Gravity Recovery and Climate Experiment
GRAS	GNSS Receiver for Atmospheric Sounding
GRO	GNSS-LEO Radio Occultation (here GPS & Galileo L band signals, ~1.2 / 1.6 GHz)
GUI	Graphical User Interface
I/F	Interface
InRet	Inversion/Retrieval, subsystem of EGOPS
IR	Infrared
L1	GPS L-band frequency at 1575.42 MHz
L2	GPS L-band frequency at 1227.60 MHz
LEO	Low Earth Orbit
LIO	LEO-LEO Infrared Occultation (here laser cross-link signals within 2–2.5 μm)
LMO	LEO-LEO Microwave Occultation (here cross-link signals within 17–23 and 178-183 GHz)

LRO	LEO-LEO Radio Occultation (alternative/earlier-used term for LMO)
l.o.s.	Line-of-sight
MAnPl	Mission Analysis Planning System, subsystem of EGOPS
Met Office	U.K. Meteorological Office
MetOp	Meteorological Operational satellite (of EUMETSAT Polar System)
MSISE-90	Mass Spectrometer-Incoherent Scatter Model–Extended version 1990
MSL	Mean Sea level (reference level for altitude and geopotential height coordinate)
NASA	U.S. National Aeronautics and Space Administration
NCEP	National Centers for Environmental Prediction
NetCDF	Network Common Data Format
OPS	Occultation Processing System
OSMod	Observation System Modeling, subsystem of EGOPS
RAER	Retrieval-to-A priori Error Ratio
RFM	Reference Forward Model
RMS	Root-mean-square
RO	Radio Occultation
S/W	Software
SAC-C	Satélite de Aplicationes Científicas-C
SAGE II	Stratospheric Aerosol and Gas Experiment II
SAM II	Stratospheric Aerosol Measurement II
SNR	Signal-to-Noise Ratio
SPARC	Stratospheric Processes And Their Role in Climate (international research program)
SWIR	Short wave infrared spectral region (1.5-3 μm; here referring to the 2–2.5 μm region)
UCAR	University Corporation for Atmospheric Research (Boulder, CO, USA)
UniGraz	University of Graz (Austria)
UTC	Universal Time Coordinated
UTLS	Upper Troposphere/Lower Stratosphere height region
WegCenter	Wegener Center for Climate and Global Change, UniGraz, Austria
WP	Work Package
zRAER50	Altitude where RAER equals 50 %

List of Symbols

α	Bending angle
$\Delta\Delta Tr_{w1w2}$	Double-difference (Tr_{w1}–Tr_{Ref}) – (Tr_{w2}–Tr_{Ref}) concerning the wind channels; also termed delta-differential transmission or delta-differential log-transmission
$\Delta Tr_{w1w2,0,Mod}$	Zero-wind transmission difference between the two wind channels
ε_a	Aerosol extinction coefficient
λ	Wavelength
v	Frequency
φ	geographical latitude
a	Impact parameter
A	Ångström exponent
$\mathbf{B}$	Background error covariance matrix
c_0	Vacuum speed of light (*SI* definition: 299 792 458 m/s)
$(\mathrm{d}Tr/\mathrm{d}v)_{wi,Mod}$	Transmission derivatives for the wind channels ($i \in \{1, 2\}$)
f	Polar oblateness (flattening)
f_s	Sampling rate
g	Acceleration of Earth's gravity
$g_{Surface}$	Earth's gravity at the surface
h	Height
hq50	Transition height between the background dominated ($\mathbf{q}_r > 0.5$) and observation dominated ($\mathbf{q}_r < 0.5$) altitude ranges
k_1, k_2	Constants in the refractivity equation
M_d	Molar mass of dry air
N	Refractivity
n	Index of refraction
$\mathbf{O}$	Observation error covariance matrix
p	Pressure (total air pressure)
p_d	Dry air pressure
p_W	Water vapor pressure
$\mathbf{q}_r$	Ratio of the diagonal elements of the retrieval error and background error covariance matrices
$\mathbf{R}$	Retrieval error covariance matrix
R	Universal gas constant
R_C	Radius of local curvature
R_{Earth}	Earth's radius
$R_{Equator}$	Earth's equatorial radius
R_{Pole}	Earth's polar radius
Ref	Index marking ACCURATE reference channels
T	Temperature
Tr	Transmission (here generally used in terms of log-transmission [dB])
V_{los}	Line-of-sight wind velocity
w1, w2	Indices marking ACCURATE wind-1 and wind-2 channel, respectively
z	Altitude over Earth's surface

(intentionally left blank; back page if double-sided print)

1 Introduction

The provision of carefully validated radio occultation (RO) climatologies from the new European MetOp satellites (MetOp-A launched in October 2006) and a range of other recent RO satellites is of key interest to climate research, since these RO observations derived from navigation signals of the Global Positioning System (GPS) allow to retrieve fundamental variables of the Earth's atmosphere (such as temperature and pressure) with unprecedented accuracy and consistency. Complementarily, preparing for future occultation systems, the ACCURATE (Atmospheric Climate and Chemistry in the UTLS Region And climate Trends Explorer) mission conceived at the Wegener Center, University of Graz (*ACCURATE*, 2005) is a next-generation climate mission concept adding independent temperature-humidity, greenhouse gas, and wind measurement information (e.g., *ACCURAID*, 2007a). Further developing this concept, and preparation of simulation tools to investigate it, is another key interest for enabling future occultation systems to provide unprecedented benchmark observations of greenhouse gas increases and related climate change.

In this context, the EOPSCLIM project contributed to software enhancement of the WegCenter's end-to-end occultation simulator and processing system ("EGOPS") along two main lines: 1) contribution to the integration of real RO data processing within EGOPS, including on the new MetOp GRAS data stream, and 2) advancement of the new ACCURATE infrared laser occultation functionality within EGOPS by aerosol modeling and by a first version of wind profile retrieval processing.

This EGOPS enhancement report describes the results of this EGOPS software advancement work under the EOPSCLIM project. Section 2, for setting the scene and providing basic EGOPS context, introduces the EGOPS software and in particular its on-going developments towards the new EGOPS6 system. Section 3 subsequently describes the results of the work on real RO data processing and Section 4 on the ACCURATE infrared laser occultation advancements. Section 5, finally provides a summary and an outlook to next steps of work.

(intentionally left blank; back page if double-sided print)

2 Overview of the EGOPS Software

In order to give a basic overview and introduction to the EGOPS software before the subsequent sections describe enhancements undertaken during the EOPSCLIM project this section gives first an overview of the EGOPS tool in its current base version EGOPS5 (subsection 2.1) and then outlines in general the context of the advancements towards EGOPS6 (subsection 2.2). The enhancements under the EOPSCLIM project are essential parts of this broader advancement towards EGOPS6.

2.1 The Simulation Tool EGOPS5

The End-to-end Generic Occultation Performance Simulator, Version 5, is a software package allowing the end-to-end simulation of GRO (GNSS-LEO Radio Occultation) and LRO (LEO-LEO Radio Occultation) measurements. Its main purpose is to support research addressing scientific and mission analysis questions on the GNSS-LEO/LEO-LEO based radio occultation technique. It is composed of a series of modules, which are integrated into so-called Systems (see Figure 2.1). The Mission Analysis and Planning (MAnPl) System allows analysis and planning of GNSS-LEO and LEO-LEO satellite constellations with regard to their suitability for occultation missions.

In particular, its main capability is that the distribution of occultation events around the globe can be simulated using arbitrary (user-generated) satellite constellations. Based on the resulting geometry data of such occultation events, the Forward Modeling (FoMod) System together with the Observation System Modeling (OSMod) System enables quasi-realistic simulation of GNSS-LEO as well as LEO-LEO radio occultation observables (i.e., phase and amplitude profiles at each signal frequency) and related required variables. In particular, FoMod's task is to simulate the electromagnetic signal propagation through the atmosphere (and ionosphere) towards the receiver based on orbital motions of transmitter and receiver satellites. The resulting occultation signals are influenced by atmospheric (and ionospheric) effects. Effects due to the receiving system (instrumental errors, in general), which usually perturb the signal quality, are superimposed during the subsequent OSMod simulation.

Finally, the Inversion/Retrieval (InRet) System is responsible for the retrieval processing of simulated or observed GRO/LRO phase and amplitude data (supplemented by the necessary geometry information) in order to obtain quasi-vertical profiles of atmospheric parameters. The retrieval algorithms for GRO and LRO differ somewhat: In the case of LRO, phase and amplitude data are converted via bending angles and transmissions down to profiles of refractivity and absorption coefficients, density, pressure (or geopotential height), temperature, and humidity (as well as liquid water if needed). In the case of GRO, only bending angles are exploited, which is why no frequency-dependent absorption coefficients can be utilized to independently retrieve humidity. A more detailed overview of the scientific retrieval algorithms for both GRO and LRO data processing is given by *Kirchengast et al.* (2004a).

The four systems mentioned above are the core of EGOPS5. Additionally, there is a so-called Visualization/Validation System, which enables post-processing of the retrieved data (statis-

tics, visualization, etc.), including the capability to extract information from the atmosphere system underlying the occultation simulations. Altogether, EGOPS5 enables research contributing to a better quantification of the potential of the GRO and LRO occultation technique for atmosphere and climate science.

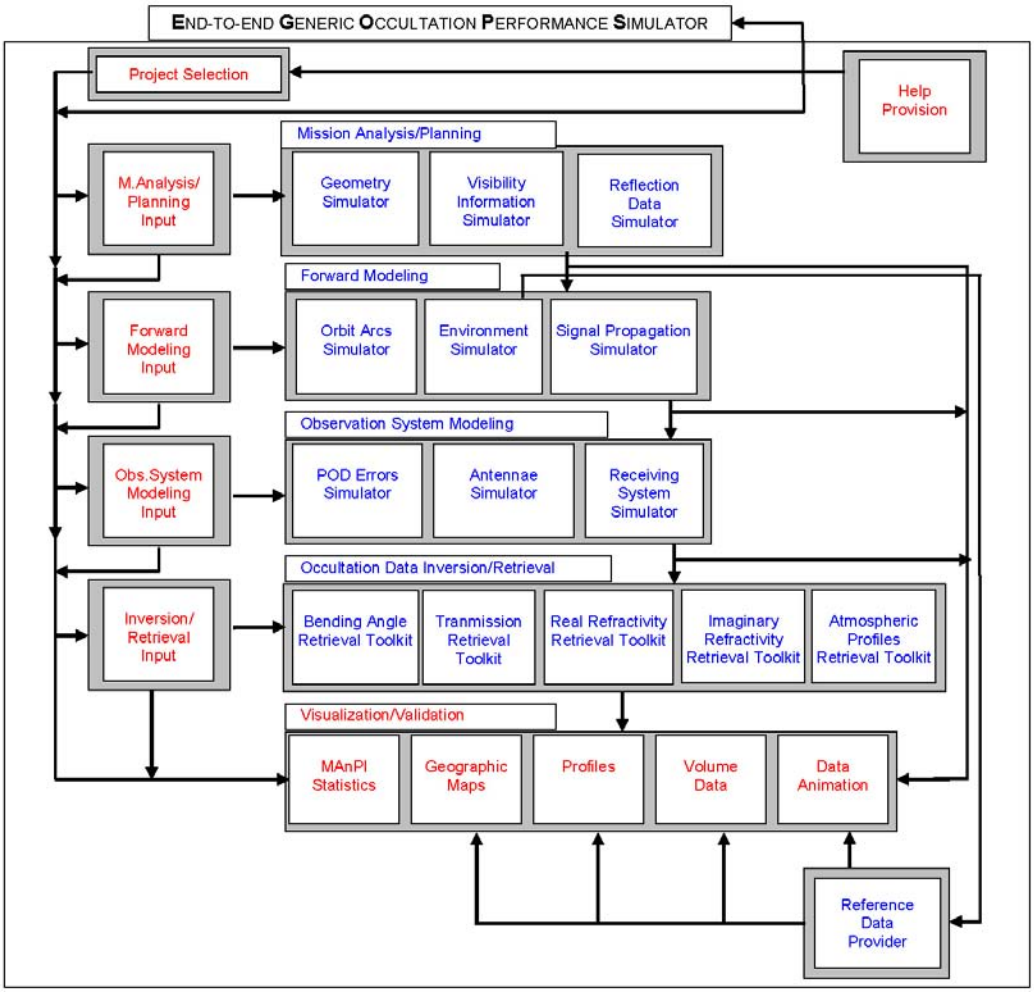

Figure 2.1: Modular view of EGOPS5 (from *Kirchengast et al.*, 2007).

2.2 Advancements towards EGOPS6

Figure 2.2 provides a schematic overview on the approach and main elements of EGOPS6. It illustrates in a system overview the EGOPS6 key dual utility for both end-to-end generic occultation simulations as well as for occultation processing of real data from GPS RO missions. The EGOPS6 simulator will combine the existing tools in EGOPS5, in concert with new ones, into a modernized and streamlined and at the same time more generic system.

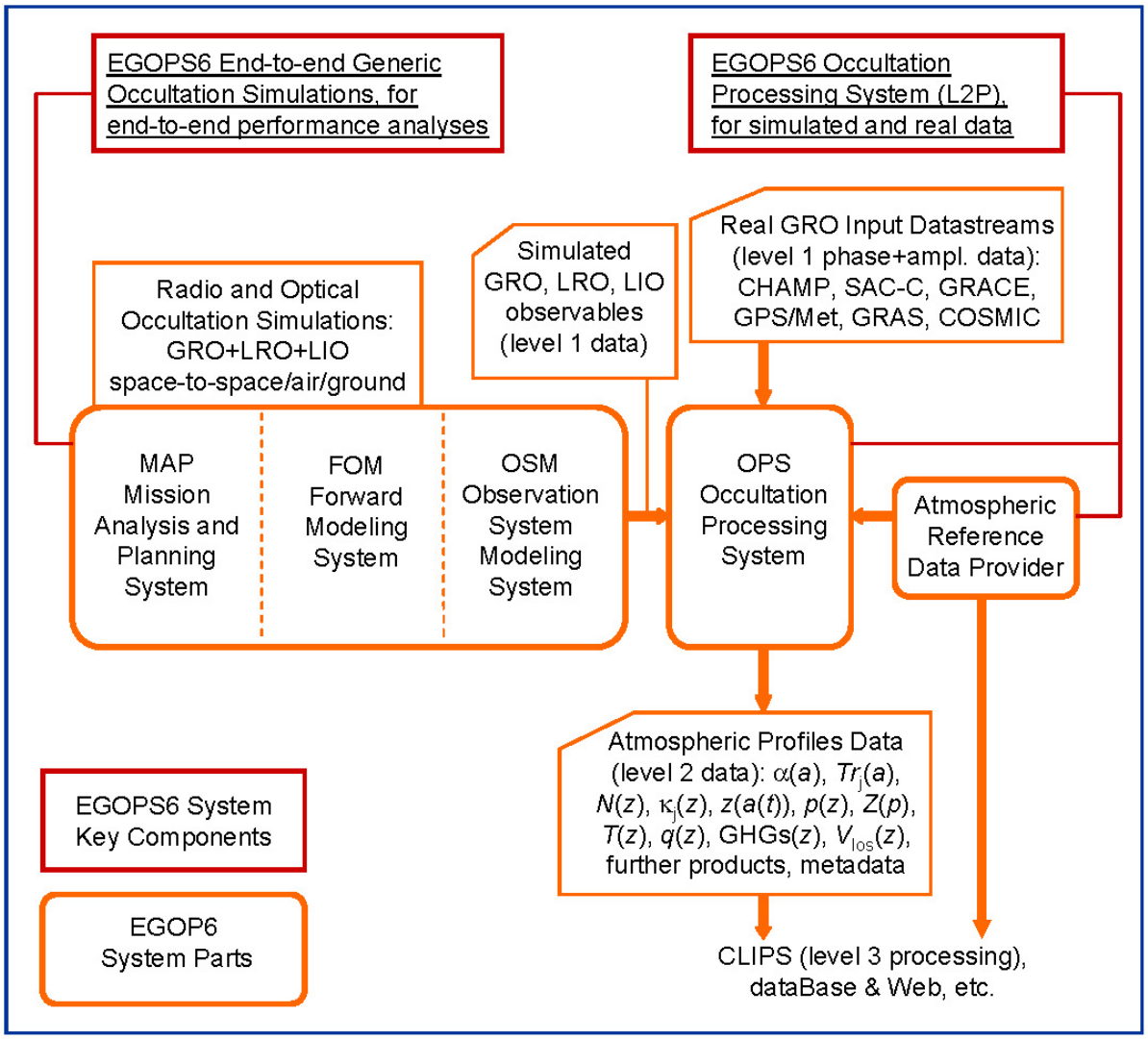

Figure 2.2: EGOPS6 Software System Overview.

More specifically, the EGOPS5 system is undergoing four vital innovations towards the new EGOPS6 system:

1) End-to-end RO simulation (GRO and LRO) and real RO data processing (GPS/Met, CHAMP, SAC-C, GRACE, COSMIC, MetOp/GRAS) – that is the current EGOPS master version (EGOPS5) and different "older" EGOPS derivatives (in particular CHAMPCLIM retrieval system CCRv2.3) – will be integrated and developed into a single system,
2) Upgrades will be provided for seamless use of space-to-ground modeling in addition to the space-to-space modeling both in the forward and observation system modeling parts, which will allow simulation of signals for space-to-ground demonstration setups similar to those for the baseline space-to-space setups,
3) End-to-end simulation of optical (infrared laser) occultation (LIO) will be integrated with radio occultation (LRO, GRO) right from the start, where in particular the integration of LRO and LIO retrieval processing system elements is a challenging part at system development level,

4) At S/W system level the EGOPS S/W interfaces, the input data I/Fs (simulated profile data file inputs, real RO mission datastreams), the output data I/Fs (performance simulation output, real data processing output), and partly the graphical user I/Fs (GUIs; such as for visualization/validation) will be streamlined to a simplified and more generic system. An automatic test suite will further enhance this innovation.

All four lines of innovation will provide a further strong boost to the scope and utility of EGOPS for all users, both internal in the Wegener Center and worldwide.

Within this EGOPS6 development context, the EOPSCLIM project was in charge of the following EGOPS enhancement aims:

1. Contribute, complementary to the parallel-running project on EGOPS Joint System Development ("ESA-Prodex project"), to the integration of the current EGOPS5 simulation system and real RO data processing (integration and advancement of CCRv2.3 retrieval system), including in particular MetOp GRAS RO datastream and processing integration.
2. Integrated into the EGOPS system, advance the new ACCURATE LEO-LEO Infrared laser Occultation (LIO) functionality in developing an aerosol model and modeling aerosol effects in LIO signal propagation, and in developing an initial LIO wind profile retrieval processing function, including an initial analysis of this new wind retrieval capability.

Below, the results of the enhancement work according to these aims 1 and 2 are described in section 3 and section 4, respectively.

3 Enhancement of the EGOPS Real GPS RO Data Processing

This section first provides (subsection 3.1) an overview of the real GPS RO data processing system at its status before integration into the new EGOPS Occultation Processing System (OPS). This was the so-called CHAMPCLIM Retrieval (CCR) system, focused at processing CHAMP RO data provided by the GeoForschungsZentrum (GFZ) Potsdam, which was at version CCRv2.3 at start of integration into EGOPS. This baseline description is then followed (subsection 3.2) by a description of the enhancements brought to the CCRv2.3 system after first integrating it into EGOPS and forming the new OPS for joint processing of both simulated and real RO phase delay and orbital data.

3.1 Overview of the CHAMPCLIM Retrieval System CCRv2.3

The CHAMPCLIM retrieval scheme (version CCRv2.3) aimed at optimal exploitation of RO data for climate research with a particular focus on avoidance of systematic errors and eventual drifts by minimizing the influence of a priori information used for initializing the retrieval at high altitudes (upper stratosphere upwards) as a potential source of temporarily inhomogeneous biases. A related aim is to minimize the amount of background information entering the retrieval process and to make the influence of the background information traceable. Based on these measures, CCR aims to extend the altitude range of reliable, accurate retrieval results (currently up to about 25 km; e.g., *Wang et al.*, 2004; *Wickert et al.*, 2004; *von Engeln*, 2006) towards the upper stratosphere (up to about 35 km). The development of the algorithmic basis and careful performance assessment via end-to-end simulation studies by *Gobiet and Kirchengast* (2004) and *Steiner and Kirchengast* (2005) have demonstrated that this improvement potential exists.

The CCRv2.3 scheme was focused on and applied to data from the first satellite providing RO measurements on a longer term, CHAMP (*Wickert et al.*, 2001; 2004), and is the basis for the first RO-based multi-year temperature climatology, which has been developed in the framework of the CHAMPCLIM project (*Foelsche et al.*, 2005; 2006), a predecessor project of the EOPSCLIM project.

3.1.1 Basic Retrieval Algorithms Employed

Basically the CCRv2.3 scheme is a so-called dry air retrieval scheme. Its basics are briefly summarized here; a detailed treatment of basic RO retrieval techniques is given in a review-type manner by *Kursinski et al.* (1997) and *Hajj et al.* (2002). The primary observables of RO measurements are phase delays of GNSS signals, i.e., the consequences of deceleration of electromagnetic wave's phase velocities by the atmosphere. Doppler shifts and subsequently the total bending angle (α) and impact parameter (a) of an occultation ray are deduced from phase delays involving transmitter and receiver orbit data using geometric optics and local spherical symmetry assumptions. Using GNSS signals from the Global Positioning System, two different carrier frequencies are available, which allow removing of large parts of the

dispersive ionospheric contribution to the signal by linear combination of bending angles of both frequencies (*Vorob'ev and Krasil'nikova*, 1994). The refractive index of the neutral atmosphere (n) can then be derived via the inverse Abel transform (*Fjeldbo et al.*, 1971),

$$n(a) = \exp\left[\frac{1}{\pi}\int_a^\infty \frac{\alpha(a')}{\sqrt{a'^2 - a^2}}\,\mathrm{d}a'\right], \tag{3.1}$$

from which refractivity as a function of height, $N(z)$, is obtained via the relation $N(a) = 10^6(n(a)–1)$ and $z(a) = a/n(a)–R_C$. R_C is the radius of curvature of the Earth along the occultation plane (*Syndergaard*, 1998). Refractivity is related to atmospheric pressure (p), temperature (T), and the partial pressure of water vapor (p_w) via

$$N = k_1 \frac{p}{T} + k_2 \frac{p_w}{T^2}, \tag{3.2}$$

where k_1 and k_2 are constants (k_1 = 77.60 K/hPa, $k_2 = 3.73 \cdot 10^5$ K^2/hPa; e.g., *Bevis et al.*, 1994).

Using the refractivity equation (Eq. 3.2), the hydrostatic equation, the equation of state, and the gravity formula, atmospheric parameters can be derived. For example, dry pressure $p_d(z)$ (which equals the total air pressure $p(z)$ if humidity can be neglected, i.e., above the middle troposphere) is obtained via hydrostatic integration,

$$p_d(z) = \frac{M_d}{k_1 R}\int_z^\infty g(z')N(z')\mathrm{d}z', \tag{3.3}$$

where R is the universal gas constant ($8.3145 \cdot 10^3$ JK^{-1}kg^{-1}), M_d is the molar mass of dry air (28.964 kg kmol^{-1}), and $g(z')$ is the acceleration of gravity. Dry temperature (which, similarly to dry pressure, absorbs the effect of water vapor) is then obtained as

$$T_d(z) = k_1 \frac{p_d(z)}{N(z)}. \tag{3.4}$$

We note that if the air is sufficiently moist so that humidity cannot be neglected, as is typically the case in the lower and middle troposphere, then temperature and water vapor can only be retrieved separately if a priori information on at least one of the two parameters is available (e.g., *Kursinski et al.*, 1997; *Healy and Eyre*, 2000). This moist air retrieval, a part of the CCRv2.3 follow-on retrieval scheme at the Wegener Center, is not further treated here since the lower and middle troposphere is below our analysis domain limited to above 10 km in this study. We thus exclusively regard dry temperature as defined above, assuming the contribution of the water vapor to be negligible, which is generally a very good assumption above 10 km (e.g., *Gobiet*, 2005).

3.1.2 Initialization and Statistical Optimization of Bending Angles

The integrate formulae, Eqs. (3.1) and (3.3), are crucial links in the RO retrieval chain. Equation (1) indicates that the inversion of bending angles leads to downward propagation of high altitude errors. Due to the localized kernel $(a'^2-a^2)^{-1/2}$ of the inverse Abel transform, this vertical correlation is limited in $N(z)$ but further and stronger error propagation occurs in the hydrostatic integration, Eq. (3.3). A detailed theoretical analysis of this error propagation has been performed by *Rieder and Kirchengast* (2001). It is thus vital to use adequate bending angles also at altitudes above any height of interest. On the other hand, since atmospheric density decreases exponentially with height and residuals from the ionospheric correction significantly disturb the RO signal above about 45 km, the high-altitude signal-to-noise ratio (SNR) is low. Without careful initialization of the two integrals, errors in temperature profiles may propagate down to 20 km or even below (*Gobiet and Kirchengast*, 2004), which are altitudes generally considered to be "optimal" for RO retrieval performance.

To cope with this problem, usually both integrals in Eqs. (3.1) and (3.3) are initialized by some kind of a priori information about the atmosphere at high altitudes. The standard approach, inherited from planetary occultation (e.g., *Fjeldbo et al.*, 1971), is to independently initialize both integrals. The Abel transform is often initialized by extrapolating the bending angle profile exponentially (e.g., *Kursinski et al.*, 1997). Since the resulting refractivity profile usually lacks quality at high altitudes, the hydrostatic integral is again initialized at some fixed altitude between 30 km and 50 km with temperature (or pressure) upper boundary "guess" value (e.g., *Kursinski et al.*, 1997; *Hajj et al.*, 2004; *Wickert et al.*, 2004), usually derived from a meteorological analysis. A modification of the extrapolation approach is statistical optimization (*Sokolovskiy and Hunt*, 1996), which optimally (in a least-squares error sense) combines the retrieved bending angle profile with a background profile from a climatology or a meteorological analysis, taking into account the error characteristics of both profiles (see *Gobiet and Kirchengast* (2004) for details). Usually, the hydrostatic integral is subsequently still initialized as described above.

Steiner and Kirchengast (2005) have, in the context of an error analysis based on ensembles of GNSS RO profiles from end-to-end simulations, discussed the weakness of the double initialization approach and found: "Regarding the climatological use of geopotential heights and temperature this approach is problematic, since it leads to intricate error characteristics and a priori dependence in the stratospheric data down to about 20 km, which threats the crucial aims of unbiasedness and a clear understanding of the degree of residual biasedness." *Gobiet and Kirchengast* (2004) presented a retrieval scheme avoiding the 2nd initialization by using full downward integration of the hydrostatic integral from 120 km in order to eliminate these problems and the related over-accentuation of a priori information in the retrieval.

Following these findings we use in the CCRv2.3 scheme a statistical optimization approach that introduces background information exclusively to the bending angles, yielding high-quality refractivity profiles up to high altitudes so that effectively no "2nd initialization" is needed to initialize the hydrostatic integral subsequently. This follows from the fact that the initialization of the hydrostatic integral with zero pressure at 120 km, compared to initialization with pressure from the MSISE-90 climatology, has no noticeable effect on the retrieved temperature profiles at any height of interest below the stratopause. 120 km can be regarded as being outside of the atmosphere from a RO retrieval point of view and effectively no fur-

ther a priori information needs to be introduced to the retrieval after statistical optimization of the bending angles. This strategy ingests less a priori information compared to most other RO retrieval schemes and allows clear tracing of the amount of non-observed information entering the retrieval (see section 3.1.3).

As has been shown by *Gobiet et al.* (2007) based on real data, rather than on simulated data as used by *Gobiet and Kirchengast* (2004), a significantly higher degree of independence from a priori information can be achieved in the critical 30 km to 40 km altitude range compared to retrieval schemes applying "2nd initialization" of the hydrostatic integral. A more detailed description of the general methodology can be found in *Gobiet and Kirchengast* (2004), its specific application to CHAMP data is described as part of the following subsection.

3.1.3 The CCRv2.3 Processing Scheme Structure and Implementation

The CCRv2.3 scheme, more precisely the dry air retrieval core scheme of interest here, starts with phase delays from CHAMP provided by the GeoForschungsZentrum Potsdam (GFZ) ("level 2 data") and returns (dry air) profiles of refractivity, density, pressure, geopotential height, and temperature, respectively. Compared to the pre-operational retrieval scheme described in *Gobiet and Kirchengast* (2004) several aspects were improved for its operational application to CHAMP data and to improve the retrieval performance. Table 3.1 below provides an overview on the main ingredients of the scheme and we briefly describe the main (improvement) aspects below; some more details are described in *Gobiet* (2005).

More stable ionospheric correction could be achieved by low-pass filtering the signals before dual-frequency correction and adding the high-pass fraction of the stronger signal afterwards (*Hajj et al.*, 2002; *Hocke et al.*, 2003). Tests identified a 1 km-width boxcar filter applied to bending angles and impact parameters being most effective, whilst broader filters created biases above 30 km and more narrow filters were less effective in terms of retrieval efficiency (i.e., a smaller number of occultation events could be successfully processed). Additionally, the retrieval quality in terms of statistical error could be slightly improved in the 15 km to 20 km altitude range.

The statistical optimization of bending angles needs an estimation of the error characteristics of the data. Unlike several retrieval schemes that use the root-mean-square (RMS) differences relative to the a priori for this purpose we derive observation errors independently from the background by analyzing the altitudinal variance of the ionosphere-corrected bending angle profiles at high altitudes, where it predominantly contains noise and the neutral atmospheric contribution to the signal is close to negligible. Compared to the RMS method, this generally reduces the observation error estimate by 10 % to 20 % (which does not necessarily mean that the lower value is more realistic). More important are single cases with severely biased background information. Depending on the quality of the background information, such cases can lead to a more than 50 % overestimation of the observation error.

Table 3.1: Overview of the CHAMPCLIM retrieval processing scheme CCRv2.3.

Early outlier rejection	"3σ " outlier rejection on 50 Hz sampling rate L1 and L2 phase delay data, based on a one-second moving window over the profile.
Phase delay smoothing	Smoothing of 50 Hz phase delay profiles using regularization (third order norm, regularization parameter = 10^5, following *Syndergaard*, 1999).
Bending angle retrieval	Geometric optics retrieval (e.g., *Kursinski et al.*, 1997) at both L1 and L2 frequencies.
Ionospheric correction	Linear combination of L1 and L2 bending angles (*Vorob'ev and Krasil'nikova*, 1994). Correction is applied to low-pass filtered bending angles (1 km moving average), L1 high-pass contribution is added after correction (*Hocke et al.*, 2003). L2 bending angles < 15 km derived via L1–L2 extrapolation.
Statistical optimization of bending angles	Statistical optimization of bending angles between 30 km and 120 km. Vertically correlated background (corr. length 30 km) and observation (corr. length 5 km) errors [preferable, though with less background stabilization, are significantly smaller corr. lengths, directly reflecting realistic error correlation structure; meanwhile used in OPSv5.4 (see section 3.2), but not yet in CCRv2.3]. Observation standard error estimated from observed variance of observed profile > 65 km. Background error: 15 %. Background information: collocated profile derived from ECMWF operational analysis (T42L60; resp. T42L91 as of 01/02/2006). Above ~60 km: MSISE-90 (*Hedin*, 1991). Optional: MSISE-90 climatology as backgr. profiles search library (following *Gobiet and Kirchengast*, 2004).
Abel transform	Numerical integration over bending angle (Simpson's trapezoidal rule) from each height (impact parameter) to 120 km. Impact parameter to height conversion with radius of curvature at mean tangent point location following *Syndergaard* (1998).
Hydrostatic integral initialization	No initialization below 120 km. At 120 km: pressure = pressure(MSISE-90).
Lower cut-off altitude	The lowermost altitude, where retrieved data is kept, is set to the altitude, where severe impact parameter ambiguities occur (impact parameter increase > 0.2 km from one data point to the next downwards).
External quality control (for outlier profiles)	Refractivity 5 km – 35 km: $\Delta N/N < 10$ %; Temperature 8 km – 25 km: $\Delta T < 20$ K. Reference: collocated ECMWF operational analysis profiles (T42L60 resp. T42L91 as of 01/02/2006).
Reference frame, vertical coordinate	Earth figure: WGS-84 ellipsoid; Vertical coordinate: mean-sea-level (MSL) altitude; conversion of ellipsoidal height to MSL altitude (at mean tangent point location) via EGM-96 geoid smoothed to 2° × 2° resolution.

The error estimation was derived from the height interval between 65 km and 80 km. Though a lower boundary of 70 km would better fulfill the low-atmospheric-signal assumption, 65 km was used in case of CHAMP as compromise for the sake of higher retrieval efficiency. Typically, the observation error standard deviation is estimated to amount to 1 μrad to 4 μrad at this altitude. For more recent RO receivers with nominally higher SNR like the GNSS Receiver for Atmospheric Sounding (GRAS) on MetOp (*GRAS-SAG*, 1998; *Loiselet et al*., 2000) or the Integrated GPS Occultation Receivers (IGOR) on the COSMIC constellation (*Rocken et al*., 2000; *Wu et al.*, 2005), it might be meaningful to raise the lower boundary.

As background information we used what we consider to be the best dataset available, the operational analyses of the European Centre for Medium-Range Weather Forecasts (ECMWF). Due to ECMWF having started RO data assimilation as of mid December 2006, CCR is scheduled to use short-range forecasts instead of analyses as a priori information beyond 2006 in order to have available sufficiently independent, yet physical consistent a priori profiles with good error characteristics (any potential influence of this change on climatology

fields will be checked). For each observed bending angle profile, one collocated set of atmospheric parameters was extracted from the temporally closest of the six-hourly ECMWF analysis fields. This was converted into a refractivity profile (Eq. 3.2), expanded upwards from ~60 km (the second-highest level of the ECMWF model) to 120 km using refractivity derived from the MSISE-90 climatology (*Hedin*, 1991) and half-Gaussian weighting (vertical scale length 7.5 km) to ensure a smooth transition, and transformed into a bending angle profile using the forward Abel transform (the inverse of Eq. (3.1); e.g., *Rieder and Kirchengast*, 2001; their Eq. 14).

The error of the background profile was assumed to amount to 15 % of the background bending angle value at each altitude, which is in reasonable agreement with the climatologic variability in the upper stratosphere and lower mesosphere and ensures that the background profile dominates only at the uppermost part of the profile, where the SNR of the observation is small (cf. also *Healy*, 2001; *Rieder and Kirchengast*, 2001). Since the bending angle in the atmosphere increases exponentially with decreasing height, the a priori error estimate grows very fast with decreasing height and is not very sensitive to the actual percentage value (values of 5 % to 20 % are commonly used and yield comparable results).

Statistical optimization restricted to altitudes above 30 km was performed using the inverse covariance weighting approach (*Healy*, 2001; *Rieder and Kirchengast*, 2001), which combines the observed and background profile in a statistically optimal way regarding their error characteristics, including vertical error correlation.

To trace errors from bending angle to temperature level in the retrieval, transformation matrices for background (**B**), observation (**O**), and retrieval (**R**) error covariance matrices ($\mathbf{R} = (\mathbf{B}^{-1} + \mathbf{O}^{-1})^{-1}$) have been implemented following *Syndergaard* (1999) as a separate diagnostic algorithm by *Gobiet et al.* (2007). That diagnostic algorithm is not part of the CCRv2.3 retrieval itself (future EGOPS OPS versions will have special error propagation diagnostics, and OPSv5.4 already has implemented one at bending angle level, see section 3.2 below) but shall be briefly commented on here to indicate its utility.

As a measure of the relative importance of the background and observed information after the statistical optimization, profiles of the square root of the ratio of the diagonal elements of the retrieval error and background error covariance matrices were analyzed ($\mathbf{q}_r$), where the retrieval-to-background error ratio $\mathbf{q}_r$ can be regarded to indicate the fraction of the retrieval error stemming from the background error following *Rieder and Kirchengast* (2001) (their Eq. 8). $\mathbf{q}_r$ allows to define background dominated ($\mathbf{q}_r > 0.5$) and observation dominated ($\mathbf{q}_r < 0.5$) altitude ranges, with the transition height (*hq50*) between these two regimes at the altitude where $\mathbf{q}_r$ equals 0.5.

In CCR temperature profiles, *hq50* typically lies between 40 km and 55 km and it lies about 4 km higher for the corresponding bending angle profiles, the actual height primarily depending on the observation error estimate for each given CHAMP bending angle profile. Two exemplary profiles, one with *hq50* = 40 km ("low" case) and one with *hq50* = 57 km ("high" case) are displayed in Fig. 1. These two cases mark the range of virtually all CCR temperature profiles for which error estimation as described above could be performed. However, about one quarter of all CHAMP phase delay profiles showed data weaknesses at high altitudes where the observation error is estimated (indicated by negative bending angles in ionosphere-

corrected bending angle profiles above some height). In these cases we down-weighted the observation by assuming a large observation error (50 μrad) which results in lowering *hq50* to about 32 km. A more sophisticated treatment of these profiles is a major possibility for further reducing the dependence of the retrieval scheme from background information (this is now part of OPS developments, see section 3.2).

After application of the inverse Abel transform, a high quality refractivity profile is available, which can be directly processed via the hydrostatic integral without adding further background information. For the sake of correctness, the integral is initialized with pressure derived from MSISE-90 at 120 km, but simply starting the integration from zero produces negligible differences in the results in the domain of interest below 50 km. Note that this does not imply that the observations significantly contribute to the retrieved temperature above about 65 km. The "effective" initialization height, where retrieved temperature essentially equals the temperature corresponding to the background bending angle profile ($\mathbf{q}_r > 0.95$), lies within about 60 km to 77 km.

Finally, a rough quality control is applied in order to remove outlier profiles featuring a relative refractivity difference greater than 10 % between 5 km and 35 km or a temperature difference greater than 20 K between 8 km and 25 km, respectively, compared to the collocated ECMWF profile. The acceptance ranges have been deliberately chosen that large (more than an order of magnitude larger than the standard errors of any of the two datasets) to ensure that indeed only severe outliers, caused by technically corrupted data, are rejected and that eventual biases in the reference dataset (ECMWF) are not introduced into the statistics of the RO retrieval results. The entire CCRv2.3 quality control system (including the rejection of technical corrupted data during the retrieval) removes about 10 % of the phase delay profiles entering the retrieval.

3.2 Enhancement of the Processing System towards EGOPS OPSv5.4

The OPS retrieval scheme, more precisely the dry air retrieval core scheme of interest here, was based on integrating the CCRv2.3 system described above into EGOPS ("OPSv5.1"). It was then improved for better operational application to CHAMP, but especially also for processing of other RO satellite data, and to deliver improved retrieval performance compared to the CCRv2.3 system. The improvements were implemented at various specific points in the system, where the very successful exploitation of the (already high quality) CCRv2.3 multi-year data record indicated further improvement potential. These enhancements are described in the following.

3.2.1 The New OPSv5.4 Retrieval in Comparison with the CCRv2.3 Retrieval

The CHAMPCLIM retrieval CCRv2.3 was purpose-built to process CHAMP radio occultation events (*Wickert et al*., 2001; 2004) but the number of satellites carrying a RO receiver and performing RO measurements increased over the last years. To name all main ones, the Argentine/US SAC-C (launch 2000) (*Hajj et al*., 2004), the German/US GRACE (launch 2002) (*Wickert et al*., 2005), the Taiwanese/US Formosat-3/COSMIC (launch 2006) (*Rocken et al*., 2000), and the European MetOp (launch 2006) (*Loiselet et al*., 2000) satellites are all able to perform RO measurements. For that reason the EGOPS software was enhanced to retrieve RO data other than CHAMP. At the same time it was possible to retrieve GPS/Met data from 1995 and 1997 (*Rocken et al*., 1997). For that reason, the software was expanded to handle different input data formats (ASCII-files and NetCDF-files) and to retrieve from rising occultation events in addition to setting occultation events.

Table 3.2 summarizes the main enhancements of the real occultation data retrieval from CCRv2.3 to OPSv5.4. In the following these enhancements are discussed in a bit more detail.

Table 3.2: Overview of the main enhancements from CCRv2.3 to OPSv5.4.

EGOPS Enhancement	OPS Version
Multi-satellite capability	OPSv5.2
Advanced outlier rejection	OPSv5.2
Smoothing of refractivity and temperature profiles	OPSv5.2
Advanced observational error estimation and initialization of bending angle profiles	OPSv5.2, OPSv5.3, and OPSv5.4
Advanced Earth figure approximation	OPSv5.2 and OPSv5.3
More consistent gravity field and vertical coordinate references	OPSv5.3
More flexible quality control	OPSv5.3
Advanced output of the processing system	OPSv5.3 and OPSv5.4

Multi-satellite capability

The OPSv5.4 retrieval is able to retrieve profiles from CHAMP and GRACE phase delay and orbital data delivered by GFZ Potsdam, from GPS/Met, CHAMP, SAC-C, and Formosat-3/COSMIC data delivered by the COSMIC Data Analysis and Archiving Center

(CDAAC) in Boulder, as well as from MetOp GRAS data delivered by the European organization for the exploitation of Meteorological Satellites (EUMETSAT). Comparisons of climatologies obtained from different satellites and different input data sources (e.g., GFZ Potsdam and CDAAC) revealed that differences in phase delay and orbit input data cause residual climatological inconsistencies. Since we use Formosat-3/COSMIC and SAC-C data provided by CDAAC in our retrieval, we also use the full record of CDAAC CHAMP data to retrieve the OPSv5.4 standard output (for illustrating the retrieval advancements of OPSv5.4 over CCRv2.3 in section 3.3.2 below we used GFZ CHAMP input data also for OPSv5.4, however, to be consistent with the earlier CCRv2.3 input).

Advanced outlier rejection

Each one-second interval of the phase delay profile is checked for data points being 3 times the standard deviation away from the mean. If so, the data point is replaced by the interval's mean. While this procedure was formerly performed separately for each one second interval it is done for a running average now.

Smoothing of refractivity and temperature profiles

A Blackman window filter was integrated in the EGOPS software to smooth the refractivity and the temperature profiles to filter the measurement's noise variability and to eliminate numerical noise (at sub-km filter width, i.e., smaller width than the ~1 km resolution of the profiles). Optionally a Hamming window filter can be used to smooth the profiles.

Advanced observational error estimation and initialization of bending angle profiles

- The error of the observed bending angles is estimated from the variance of the observed profile within the impact height interval from 65 km to 80 km. While the mean profile was estimated by a linear or exponential fit in the past, a MSISE-90 shaped fit to the profile is used now, which results in improved robustness and adequacy of error estimates.
- An accurate analysis of bending angle profiles detected invalid data in some profiles below an impact height of 50 km. Discarding these "bad" profiles had a relatively large impact from the climatologic point of view, i.e., improved quality control. The climatologic standard deviation and the systematic difference to climatologies derived from ECMWF was considerably decreased (particularly) at high latitudes.
- Since December 12, 2006, the ECMWF assimilates GPS RO measurements (*ECMWF* 2006, *Healy* 2007) rendering the operational ECMWF analyses not independent of RO profiles any more. In order to maintain independence of RO measurements themselves, we now use ECMWF short-range forecast profiles as background in the statistical optimization. ECMWF forecasts are always run at midnight and noon. To obtain ECMWF forecast data at four equally distributed time layers (00 UTC, 06 UTC, 12 UTC, and 18 UTC) we extract 24 hr (yielding the 00 UTC and 12 UTC time layer) as well as 30 hr forecasts (yielding the 06 UTC and 18 UTC time layer) with a resolution of ~2.5° x 2.5°, matching the horizontal resolution of near 300 km of the RO measurements.
- To allow more independence of the retrieved profiles from the background profiles after the statistical optimization, we decreased the correlation length by a factor of three. The correlation length of the observed profile now is set to 2 km while the correlation length of the background profile is set to 10 km, reasonably representing expected actual correlations in these respective data. Due to these correlation length

changes the systematic differences to ECMWF increased particularly at altitudes above 30 km. *Gobiet et al.* (2007) found a consistent cold bias above 35 km between CHAMP CCRv2.3 data and GEOS-4 (Goddard Earth Observing System), CHAMP and Met Office, and CHAMP and NCEP/CPC (National Centers for Environmental Prediction/Climate Prediction Center) data. They assumed this cold bias to be caused by CHAMP data being somewhat too cold resulting from the statistical optimization with too cold ECMWF data. After the enhancement to OPSv5.4, RO temperature profiles are now somewhat warmer above 25 km to 30 km and more consistent with these other independent atmospheric analyses.

- As additional information to the bending angle profile we write the Retrieval to A priori Error Ration (RAER) to the output file to better judge the characteristics of the retrieved bending angle. It is a measure of the relative importance of the background and observed information after the statistical optimization. RAER, given in percent, allows to define background dominated (RAER>50 %) and observation dominated (RAER<50 %) altitude ranges. At the transition height (zRAER50) between these two regimes the RAER equals 50 %.

More consistent Earth figure approximation

In CCRv2.3 the Earth's radius R_{Earth} was approximated by

$$R_{\text{Earth}} = R_{\text{Equator}} \cdot \left(1 - f \cdot \sin^2 \varphi\right) ,$$

where R_{Equator} is the equatorial radius, f the polar oblateness ($f = (R_{\text{Equator}} - R_{\text{Pole}})/R_{\text{Equator}}$), and φ the geographical latitude. This approximation was replaced in the OPSv5.4 retrieval by the implementation of the general ellipsoidal equation in polar coordinates:

$$R_{\text{Earth}} = \frac{R_{\text{Equator}} \cdot (1 - f)}{\sqrt{1 - f \cdot (2 - f)\cos^2 \varphi}} .$$

At 45° latitude, where the difference is most pronounced, the correction amounts to about 27 m. The better Earth figure approximation thus improved the absolute altitude accuracy.

More consistent gravity field and vertical coordinate references

The approximation of the Earth's surface gravity field ($g_{\text{Surface}}(\varphi) = 9.7803 \cdot (1+0.0053 \sin^2\varphi)$) (*Gobiet* 2005) was replaced by the implementation of the International Gravity Formula:

$$g_{\text{Surface}}(\varphi) = 9.780327 \cdot \left(1 + 0.0053024 \cdot \sin^2 \varphi - 0.0000058 \cdot \sin^2 (2\varphi)\right) .$$

The Earth's gravity g at (ellipsoidal) height h is calculated from

$$g(\varphi, h) = g_{\text{Surface}}(\varphi) \cdot \frac{(R_{\text{Earth}})^2}{(R_{\text{Earth}} + h)^2} .$$

The gravity is now also consistently referred to the (WGS84) ellipsoid, while (MSL) altitudes, and geopotential heights, are consistently related to the geoid (2° x 2° smoothed

EGM96, see Table 3.1). These improvements in particular aided the absolute accuracy of geopotential height leveling.

More flexible quality control

External quality control of radio occultation data (refractivity and temperature profiles) can optionally be performed using either ECMWF analysis or ECMWF forecast data as co-located quality control background profiles; in CCRv2.3 it was only possible based on ECMWF analysis data. Default used in OPSv5.4 is still ECMWF co-located analysis profiles since this is computationally faster in the current setup.

Extended output of the processing system

- The retrieved bending angle profile, the RAER profile, and the ECMWF profile used in the statistical optimization process, are an additional output as a function of impact altitude (related to impact parameter). The impact altitude is the impact parameter minus the local radius of curvature minus the geoid undulation. The impact altitude grid is consistent with the mean-sea-level altitude grid which is the vertical coordinate of retrieved meteorological parameters (refractivity, density, pressure, temperature). The reference bending angle profile is provided on the same impact altitude grid as the retrieved bending angle profile.
- As reference data we use what we consider to be the best dataset available, the operational analyses of the ECMWF (T42L60 resp. T42L91 as of February 1, 2006). For each observed profile, one co-located set of atmospheric parameters is extracted from the temporally closest of the six-hourly ECMWF analysis fields. We compute and extract reference data not only for refractivity, pressure, geopotential height, temperature, and dry temperature (as in CCRv2.3) but in addition for dry pressure, dry geopotential height and humidity. Together with the dry temperature profile (or the refractivity profile), the humidity profile allows the estimation of the physical temperature profile and of the physical pressure and geopotential height profiles as well. For each reference profile (all of them reach down to the Earth's surface) the tropopause parameters are derived.
- The set of surface parameters (geoid undulation, surface altitude, surface temperature, surface humidity, surface pressure, skin temperature) is extended by the surface geopotential height.

3.2.2 Results of the Retrieval Enhancements for an Example Month

To illustrate the enhancements, Figures 3.1, 3.2, 3.3, and 3.4 depict retrieved CHAMP climatologies (excess phase delay and orbit data source: GFZ Potsdam) and their standard deviations, systematic differences, and sampling errors of refractivity, dry pressure, dry geopotential height (without sampling error), and dry temperature, respectively. April 2002 has been chosen as example month and is well representative of any other monthly climatology. The left columns show the climatologic results derived from the CCRv2.3 retrieval, the right columns represent the climatologic results derived from the new OPSv5.4 retrieval.

The main advancements, in terms of data quality, of the OPSv5.4 retrieval are:

1. A smaller standard deviation of all retrieved parameters, particularly at high altitudes; this was mainly achieved by selectively discarding profiles whose bending angles

contained invalid data below 50 km.

2. The disappearance of the feature remembering a butterfly, best visible in the systematic difference in refractivity, pressure, and geopotential height; it was caused by the insufficient approximation of the Earth's figure. This insufficient approximation had, however, only insignificant effect on dry temperature results (see Fig. 3.4), which have been used so far for several publications based on CCRv2.3 dry temperatures. The reason is that the systematic errors in refractivity and pressure largely cancel when computing dry temperature.

3. A greater systematic difference between RO and ECMWF in pressure, geopotential height, and temperature above 25 km to 30 km. The reason is the smaller correlation lengths used in the statistical optimization procedure, allowing the retrieved profiles to deviate more from ECMWF which is likely more realistic (as ECMWF is found, from various validation studies, to have a cold bias relative to actual temperatures above 25 km to 30 km; see, e.g., *Gobiet et al.*, 2007).

4. An insignificantly larger sampling error, which results from the slightly smaller number of measurements incorporated in the climatologies (RO profiles with bad values below 50 km are additionally discarded in OPSv5.4).

In summary, as Figures 3.1 to 3.4 indicate, the integration of real GPS RO data processing into EGOPS and the subsequent enhancements to OPSv5.4 were successful. The integration also greatly facilitated further planned enhancements, where in particular advancement towards climate-quality moist air retrieval in the troposphere (including humidity retrieval) from real GPS RO data is an essential and promising next step.

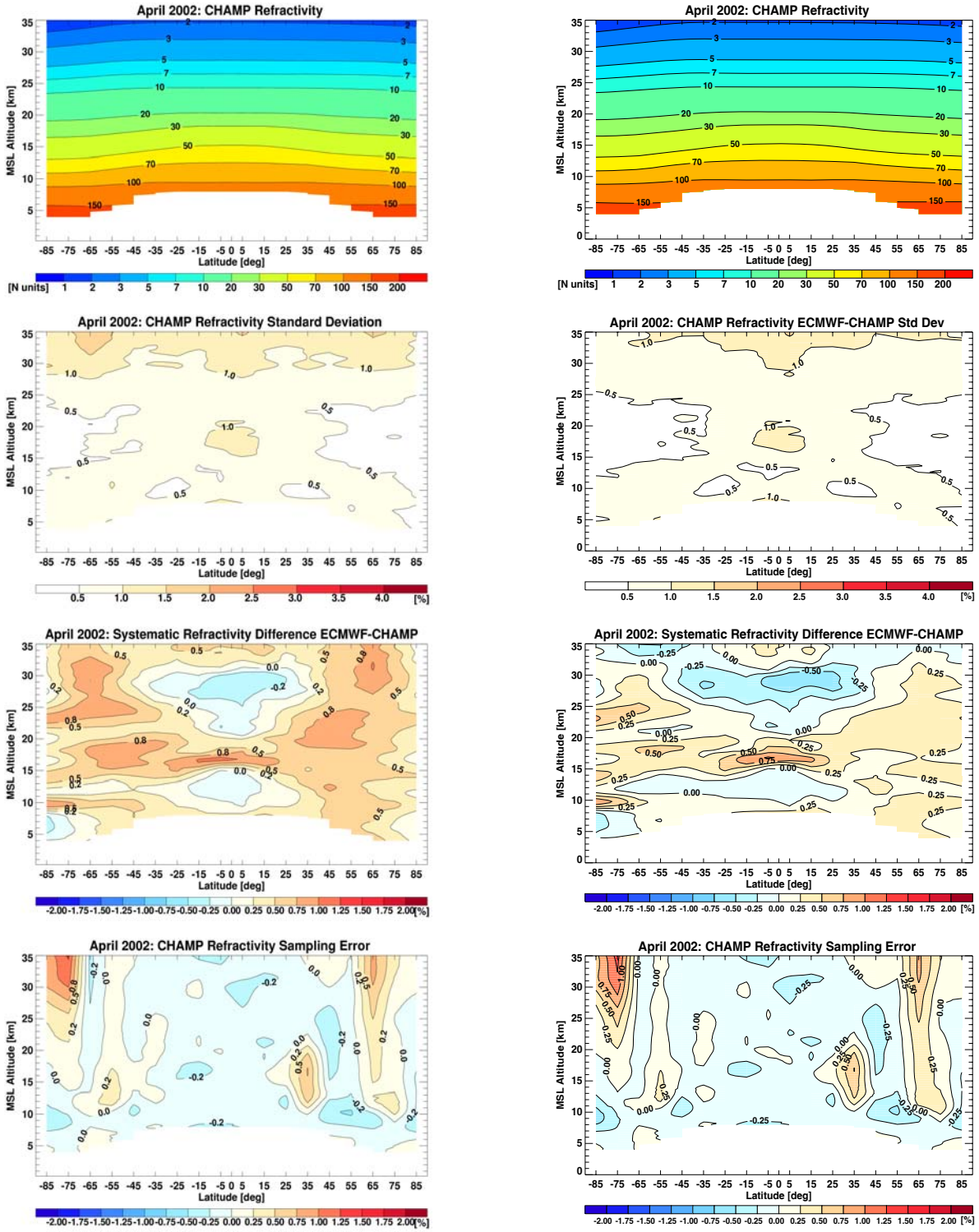

Figure 3.1: Climatologies, standard deviation, systematic difference to ECMWF, and sampling error of refractivity determined by the CCRv2.3 retrieval (left) and the OPSv5.4 retrieval (right). (The CCRv2.3 plots here, from an earlier plot program version which was meanwhile improved, show contour labels with only one post-comma-digit also for the "quarter contours", i.e., 0.2 for 0.25, 0.7 for 0.75, etc.; but note that the associated color bar shows the correct full labeling.)

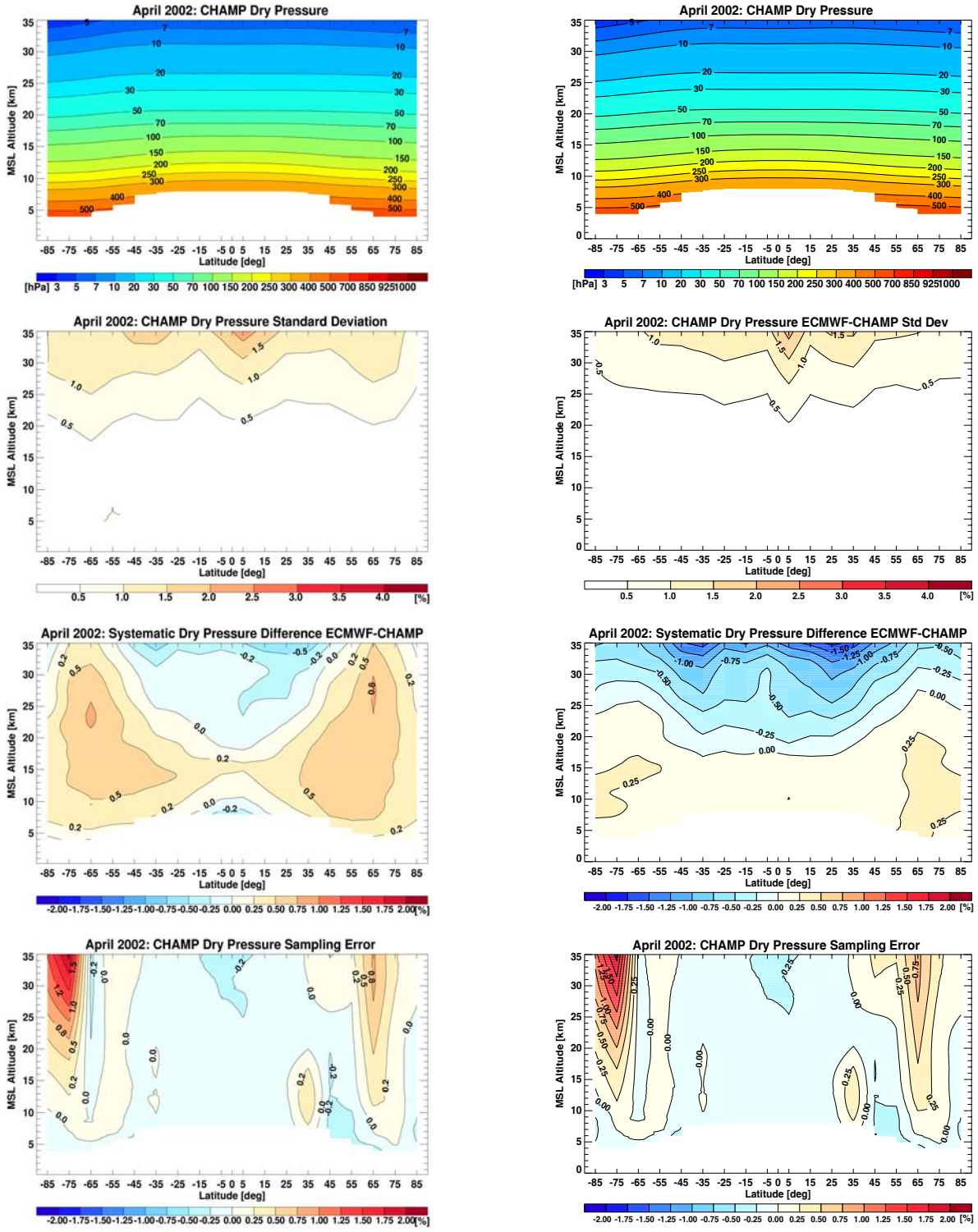

Figure 3.2: Climatologies, standard deviation, systematic difference to ECMWF, and sampling error of dry pressure determined by the CCRv2.3 retrieval (left) and the OPSv5.4 retrieval (right). (The CCRv2.3 plots here, from an earlier plot program version which was meanwhile improved, show contour labels with only one post-comma-digit also for the "quarter contours", i.e., 0.2 for 0.25, 0.7 for 0.75, etc.; but note that the associated color bar shows the correct full labeling.)

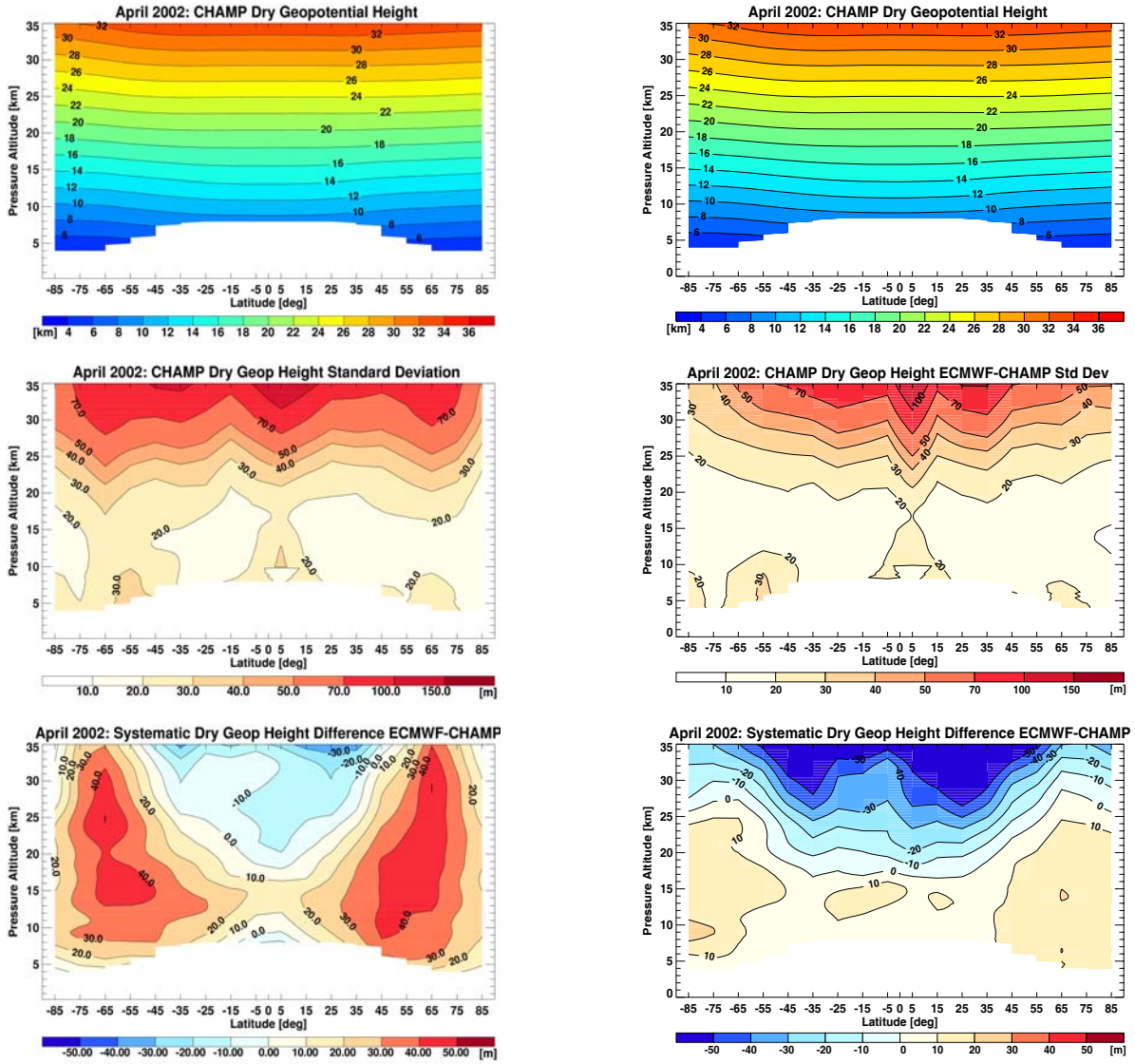

Figure 3.3: Climatologies, standard deviation, and systematic difference to ECMWF of dry geopotential height determined by the CCRv2.3 retrieval (left) and the OPSv5.4 retrieval (right). (Sampling error is not shown for this parameter, since a geopotential height reference field processing element is not yet part of EGOPS but soon implemented in a separate on-going project.)

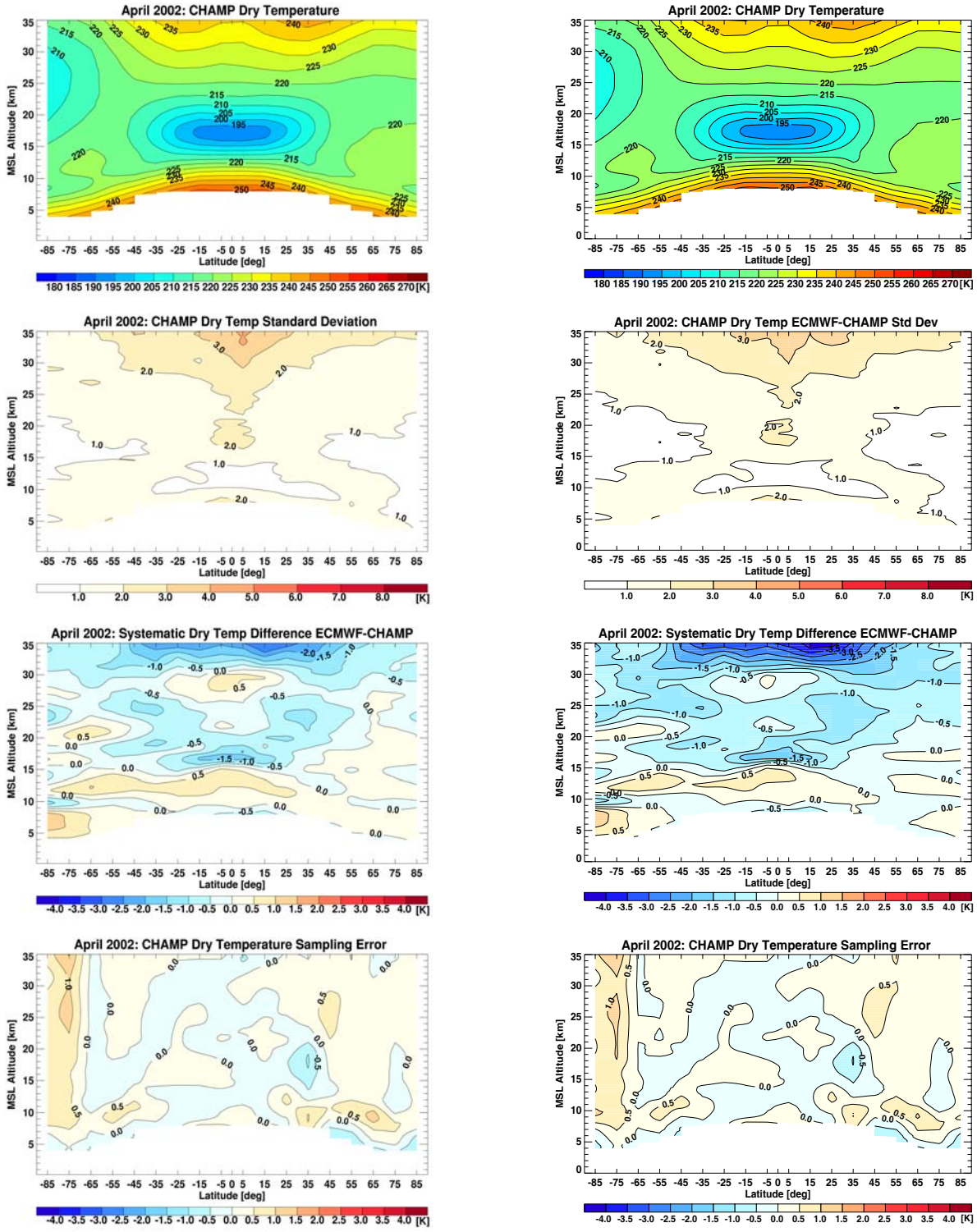

Figure 3.4: Climatologies, standard deviation, systematic difference to ECMWF, and sampling error of dry temperature determined by the CCRv2.3 retrieval (left) and the OPSv5.4 retrieval (right).

4 Enhancement of EGOPS IR Laser Occultation Capabilities

This chapter describes the enhancements of EGOPS done within the scope of the EOPSCLIM project concerning the infrared forward modeling and retrieval part. Regarding the forward modeling part, a two-dimensional atmospheric aerosol model was developed (besides the already existing one-dimensional simple aerosol model) and the appropriate forward modeling capabilities were established so that it is now possible to simulate the effects of aerosols on propagating SWIR frequencies. Details on the implementation and first simulation results are presented in subsection 4.1. Regarding the retrieval part, an initial approach for the retrieval of wind velocity in line-of-sight direction of an occultation event from SWIR signals was developed. The details of this simple local wind retrieval are described in subsection 4.2.

4.1 Development of an Aerosol Model based on SAGE II Measurement Data

This subsection contains details on the development of the two-dimensional atmospheric aerosol model of EGOPS, which is mainly based on SAGE II measurement data, and shows first results of propagation modeling of SWIR signals through aerosol laden air. Subsection 4.1.1 contains overall information on the database which was used for the development of the aerosol climatologies which served as basis for the EGOPS aerosol model. The development process of these basic climatologies is depicted in subsection 4.1.2. Subsection 4.1.3 explains the integration of the aerosol model into EGOPS and subsection 4.1.4 shows first simulation results.

4.1.1 The SAGE II Aerosol Extinction Database

The Stratospheric Aerosol and Gas Experiment II (SAGE II) is an instrument aboard the Earth Radiation Budget Satellite (ERBS) of NASA. SAGE II measures sunlight through the limb of the Earth's atmosphere, i.e., in occultation geometry, in seven spectral wavelengths from 385-1020 nm. From scattering and absorption of the sunlight by trace gases and aerosols, vertical profiles of ozone, water vapor, nitrogen dioxide and aerosol concentrations may be derived. This measurement principle is almost the same as applied by the LIO part of the ACCURATE mission with the crucial difference that LIO uses artificial light sources which may be adjusted to and selected dependent on the measurement requirements. A variety of trace gases may thus be detected via selection of signal frequencies, which are absorbed by these gases. The power of the signals in use must and can be adjusted to the expected absorption of the signal in order to ensure an exploitable SNR at the receiver. This possibility for adjustment of power is one of the main advantages of artificial light sources compared to natural light sources like the sun (besides, for example, the independency on day and night and the possibility for selection of arbitrary wavelengths).

Concerning aerosols, SAGE II measures the atmospheric aerosol extinction coefficients at different wavelengths. The aerosol extinction coefficients derived from the channels at 525 and 1020 nm are reasonably suited for being used as basis for an aerosol model valid from 500 nm up to the upper end of the SWIR spectral range (2000-2500 nm, the core spectral

range of the LIO part of ACCURATE). The reason for this basic suitability is that the spectral distance between 525–1020 nm and the SWIR range is still small enough so that aerosol extinction is expected to have similar properties in both ranges, which allows scaling of the extinction from 525 nm and 1020 nm to the higher wavelengths within the SWIR range. Clearly details of the (unknown) actual aerosol particle distribution as function of wavelength will limit the absolute extinction coefficient accuracy dependent on atmospheric conditions. But in average the SWIR estimates should be of the right magnitude or tentatively conservative if the particles' spectral distribution strongly depletes at wavelengths from 1μm towards 2 μm.

Thus we used the SAGE II aerosol extinction measurements at these two channels to construct the EGOPS aerosol model. Since the raw SAGE II aerosol extinction coefficient measurement data have major gaps, we used a pre-worked database from *Thomason and Peter* (2006), which is freely available after simple online registration via the SPARC Data Center website (*SPARC*, 2008). Thomason and Peter developed a complete, nearly gap-free aerosol extinction coefficient database including latitudinal-height resolved (80°S–80°N in 5° steps, 5–39.5 km in 0.5 km steps), monthly-mean aerosol extinction coefficients from 1979 to 2004 derived from SAM II, SAGE I, SAGE II and SAGE III measurements (see Fig. 4.1). The basic dataset was the SAGE data and gaps were filled using SAM II and a variety of lidar data sets. A detailed description of the development of this aerosol database may be found in *Thomason and Peter* (2006).

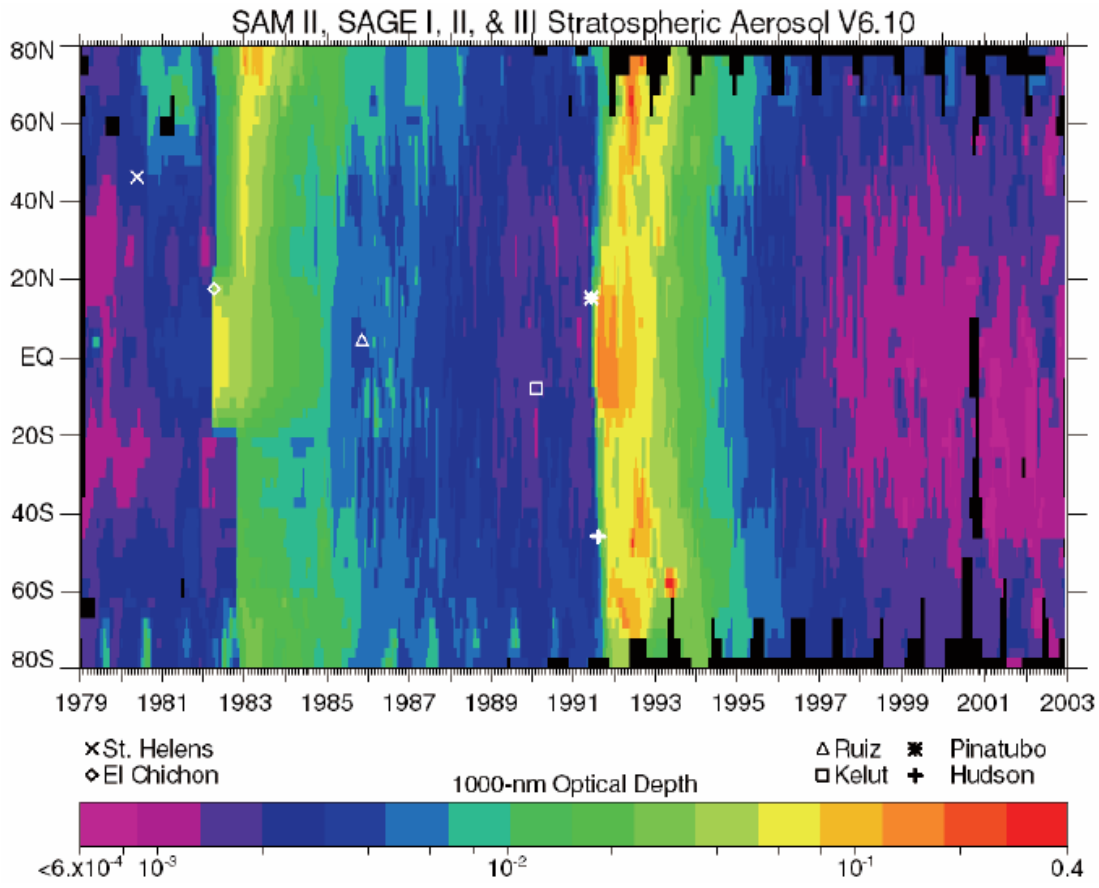

Figure 4.1: Time series of aerosol optical depth (vertically integrated aerosol extinction coefficients) at 1000 nm recorded by SAM II, SAGE I, II, and III for 1979–2002 in which data gaps have been filled. The symbols indicate volcanic eruptions (from *Thomason and Peter*, 2006).

4.1.2 Development of the Tabular Climatologies used in the Atmospheric Aerosol model

Starting with the database of Thomason and Peter (cf. subsection 4.1.1) we developed tabular climatologies of aerosol extinction coefficients at 1020 nm and 525 nm for background, medium and volcanic aerosol load. Initially it was planned to develop seasonally dependent climatologies for these three aerosol loads, but the seasonal variation of the extinction coefficients was found out to be reasonably small to be disregarded. The development of the climatologies included steps as follows.

First, the raw data of Thomason and Peter were screened for outlier values, which were then set to physically reasonable values. An investigation of the data showed that such a physically reasonable upper boundary for large extinction coefficients is 0.03 km^{-1} (valid for 1020 nm and 525 nm). At polar latitudes beyond 50°N and 50°S, respectively, the upper boundary was found more adequate at 0.005 km^{-1} and thus set to this value. Afterwards, remaining gaps were filled via log-linear interpolation in latitude (i.e., at given height levels). If boundary values were missing, the last reasonable value of a height was continued through all latitudes up to the highest latitude (north and south). The same principle was applied to extend the raw data from 80°S/80°N to 90°S/90°N. Concerning the height range, the data were extrapolated at the upper end by half a kilometer up to 40.0 km, assuming a log-linear decrease of the aerosol extinction coefficient (to have a complete 5.0–40.0 km height range as basis).

These first steps led to a totally gap-free raw database, which was then used for the development of the tabulated aerosol extinction coefficient climatologies.

In order to be able to compare the influence of various aerosol loads on the propagation of SWIR signals, we selected three periods of time in which aerosol load differed significantly. One period contains a very high aerosol load induced by large volcanic eruptions (“volcanic aerosol load”), the second period contains medium aerosol load being representative for the recovery period after big volcanic eruptions (“medium aerosol load”), and the third period contains low aerosol load being representative for air free from volcanic aerosol (“background aerosol load”). Considering Fig. 4.1 it is obviously a reasonable choice that the period from Jan. 1992 to Dec. 1993 is appropriate for the volcanic, Jan. 1995 to Dec. 1997 for medium, and Jan. 1999 to Dec. 2004 for the background aerosol load. Since the data in these periods are dominated by SAGE II measurements, we called our model “SAGE II based Atmospheric Aerosol Model”.

The tabular climatologies within these periods were derived from the gap-free database as follows. First, the average monthly-mean aerosol extinction of a period was computed via averaging the extinction coefficients within the respective months of all years. Afterwards, these average monthly-mean climatologies for background, medium and volcanic aerosol load were compared to each other and it was ensured that the volcanic average monthly-mean climatologies thoroughly contain only equal or higher values than the medium climatologies, and the medium climatologies thoroughly contain only equal or higher values than the background climatologies. That is values in the medium case, which were smaller than in the background case were set to the respective background value. Likewise, volcanic values smaller than the corrected medium values were set to the corrected medium values. After-

wards, these corrected climatologies were slightly smoothed applying a 3-point (10°) Hamming filter over latitudes and a 5-point (2 km) Hamming filter over heights.

Finally, the corrected and smoothed average monthly-mean aerosol climatologies were averaged over all twelve months of the year, resulting in the three selected-period-mean atmospheric aerosol extinction climatologies representative for background, medium and volcanic aerosol load, respectively (shown in Fig. 4.2).

The additional parameter needed and estimated was the Ångström exponent. The Ångström exponent describes the dependence of the aerosol extinction coefficient on the wavelength and it is needed for the development of the atmospheric aerosol model based on climatologies in order to be able to scale the extinction coefficients from the tabulated wavelengths to the desired wavelength. The formula for estimating the Ångström exponent is as follows:

$$\varepsilon_{\mathrm{a}}[\mathrm{m}^{-1}] = \varepsilon_{\mathrm{a},\lambda 0}[\mathrm{m}^{-1}] \cdot \left(\frac{\lambda_0}{\lambda}\right)^{A}, \tag{4.1}$$

where ε_{a} and $\varepsilon_{\mathrm{a},\lambda 0}$ are the aerosol extinction coefficients at two different wavelengths λ and λ_0, respectively, and A is the Ångström exponent. We exploited this relation in order to compute a field of latitudinal-height resolved Ångström exponents from the climatologies at 1020 nm and 525 nm representing the background aerosol load (since this is the most representative case for the wavelength dependence of the aerosol extinction coefficient towards 2–2.5 μm, because the particle spectral distribution of aerosols is regular in background aerosol load) as follows:

$$A = \frac{\ln(\varepsilon_{a,525} / \varepsilon_{a,1020})}{\ln(\lambda_{1020} / \lambda_{525})} . \tag{4.2}$$

The resulting field of the Ångström exponent as well as the climatologies of the 1020 nm aerosol extinction coefficient for the background, medium, and volcanic aerosol load are shown in Fig. 4.2. These are the basis for the SAGE II based atmospheric aerosol model of EGOPS, which is applicable between 500 nm and 2500 nm (formally, but not recommended, also up to 5000 nm).

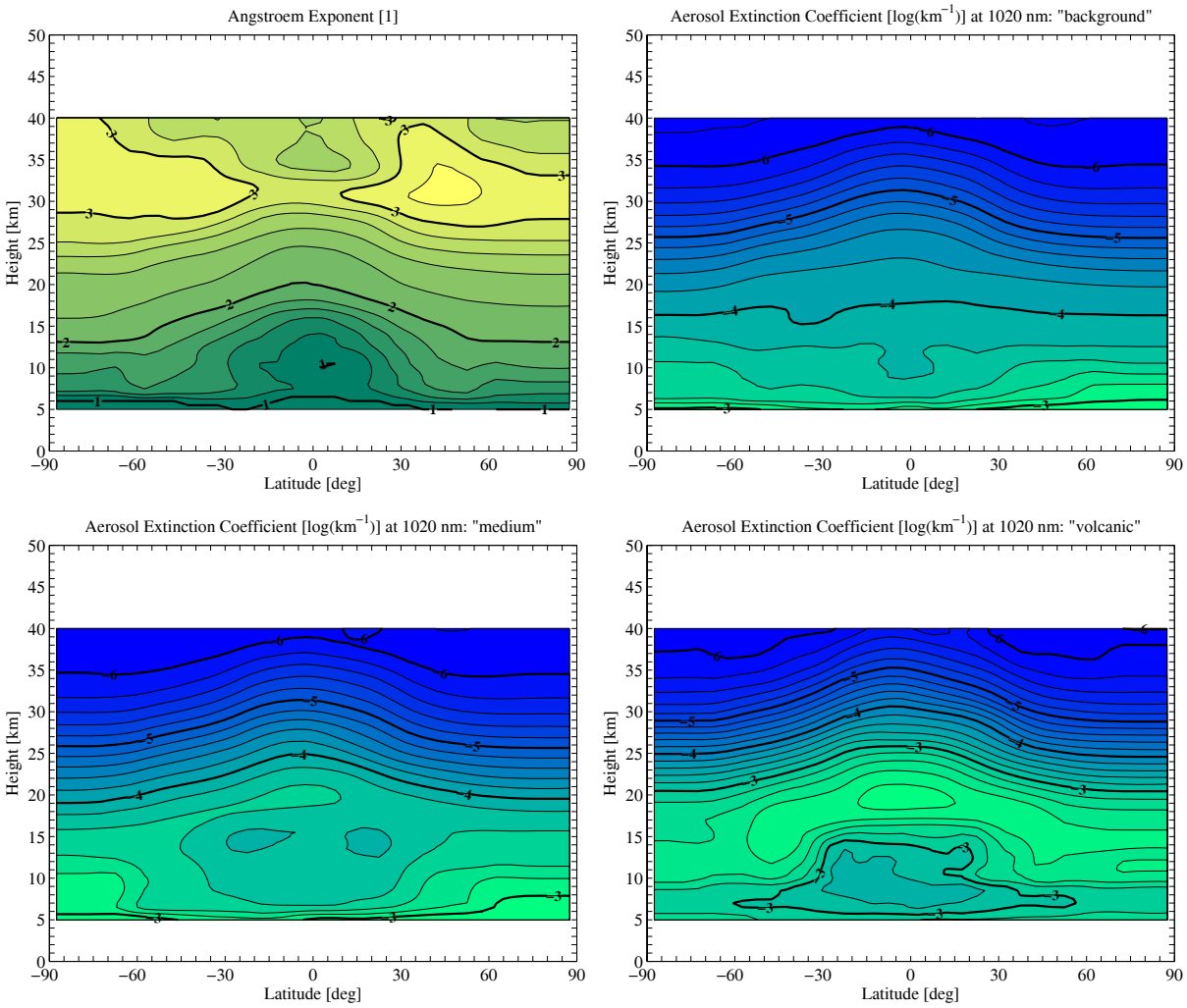

Figure 4.2: The basis for the SAGE II based atmospheric aerosol model of EGOPS: Angström exponent field (upper left) and aerosol extinction coefficient climatology at 1020 nm for background (upper right), medium (lower left) and volcanic (lower right) aerosol load.

4.1.3 The SAGE II-based Aerosol Model of EGOPS (HLatAerosolExtinctionModel)

HLatAerosolExtinctionModel is a Fortran-90 module, which implements a two-dimensional model of the atmosphere's annual-mean aerosol extinction coefficient based on tabular SAGE II aerosol data prepared as described in the previous subsection 4.1.2. Generally speaking, the model computes the aerosol extinction coefficient (in km^{-1}) for given values of latitude (in deg), height (in km), frequency (in Hz) and aerosol load ("background", "medium", or "volcanic") using one of three different interpolation methods. These are:

- linear interpolation in vertical and latitudinal direction
- natural cubic spline and linear interpolation in vertical and latitudinal direction, respectively
- natural cubic spline interpolation in vertical and latitudinal direction

The individual choice of the interpolation method to be applied reflects the trade-off between efficiency and accuracy: If maximum efficiency is expected from the model, linear interpolation should be selected. Otherwise, if the model result is required to be accurate spline interpolation should be chosen.

The source code of the HLatAerosolExtinctionModel module is structured into four procedures:

- Run_HLatAerosolExtinctionModel – provides the API
- Read_SAGEIIFile – reads the SAGE II aerosol database into memory
- Prepare_AerosolData – accomplishes preparative computations
- ExtinctCoeff – interpolates the aerosol extinction coefficient

With the exception of the top-level subroutine Run_HLatAerosolExtinctionModel, none of these procedures is accessible from outside the module.

Upon invocation, subroutine Run_HLatAerosolExtinctionModel verifies the validity of the values referenced by the latitude, height, and frequency arguments. Providing these values lie in the respective allowable ranges (i.e., $-90 \text{ deg} \le \varphi \le +90 \text{ deg}$, $h \ge 0$ km, and 6.0E+13 Hz $\le \nu \le$ 6.0E+14 Hz), execution continues by calls to the private Read_SAGEIIFile, Prepare_AerosolData, and ExtinctCoeff procedures. Otherwise, flow of control is immediately returned to the calling scope together with a specific invalid value for the aerosol extinction coefficient.

Function Read_SAGEIIFile reads the SAGE II aerosol database into memory. On disk, the SAGE II aerosol database is represented by two ASCII files, the first containing a latitude-height table of the Ångström exponent and the second containing reference latitude-height tables of the "background", "medium", and "volcanic" aerosol extinction coefficients at 1020 nm (the data illustrated in Fig. 4.2). The grid underlying the latitude-height tables covers latitude values between –87.5 deg and +87.5 deg ($\Delta\varphi$ = 5 deg) and height values between 5 km and 40 km (Δh = 0.5 km). In memory, the arrays storing the latitude-height tables are appended by two additional artificial rows at –92.5 deg and +92.5 deg which constitute simple copies of the rows at –87.5 deg and +87.5 deg, respectively. This is done in order to avoid subsequent need for latitudinal extrapolation even if values up to the poles are requested.

Subroutine Prepare_AerosolData performs three computational tasks that have to be completed before the aerosol extinction coefficient can be interpolated to the given values of latitude and height. First, the reference aerosol extinction-coefficient table residing in memory is mapped to the desired frequency by means of the Ångström-exponent table according to Eq. (4.1) of the previous subsection 4.1.2. Secondly, the second derivatives of the mapped aerosol extinction-coefficient table with respect to latitude and height are constructed insofar as they are required by the spline interpolation performed in the subsequent ExtinctCoeff procedure. Thirdly, two scale heights are estimated capturing the assumed exponential increase and decrease of the aerosol extinction coefficient below 5 km and above 40 km, respectively.

Finally, function ExtinctCoeff calculates the aerosol extinction coefficient at the specified latitude-height location by applying the selected interpolation method. The basic interpolation algorithms employed are, essentially, the standard algorithms that are defined and used by the CIRA-86 based composite atmosphere model (CIRA86aQ) of the EGOPS system (*Kirchengast et al.*, 1999). Below 5 km and above 40 km, the aerosol extinction coefficient is exponentially extrapolated, relying on the two scale heights estimated by the preceding Prepare_AerosolData procedure. In case of spline interpolation, a continuous transition is preferable between the spline interpolate and the exponential extrapolate up to the first derivative with respect to height. This is achieved using an adequately parameterized half-Gaussian function.

Figure 4.3 illustrates representative results from HLatAerosolExtinctionModel for the ACCURATE CO_2 line center channel (near 2.1 μm), in order to indicate the correctness and reasonableness of the model implementation (produced by spline interpolation). The following subsection 4.1.4 further shows, based on realistic occultation signal propagation simulations by EGOPS, how atmospheric transmission profiles are affected by different aerosol loads.

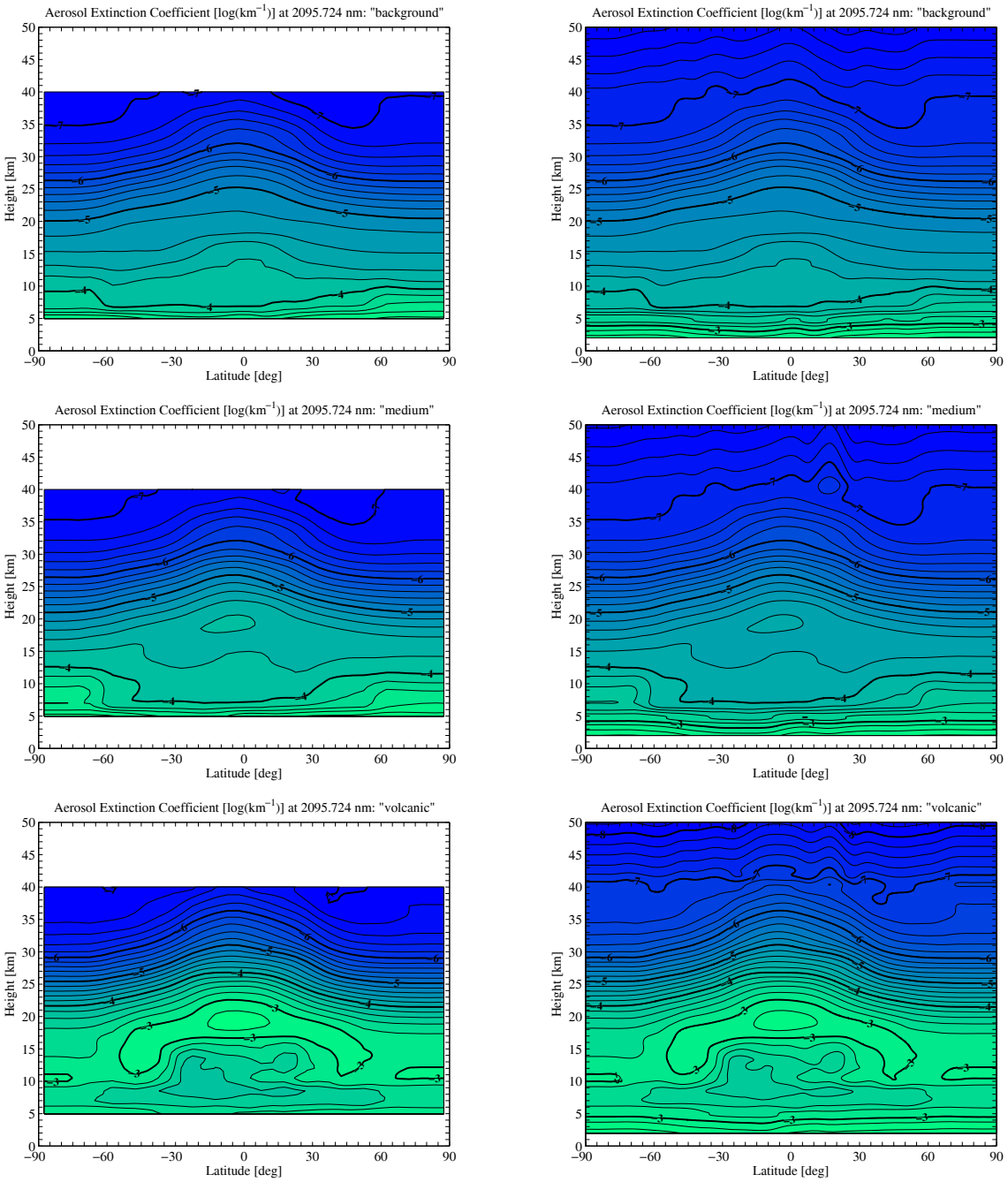

Figure 4.3: Overview on aerosol extinction coefficient model fields at the ACCURATE CO_2 line center frequency near 2.1 μm both at the native grid (left column; same 5° x 0.5 km grid as for the basic tables presented in the previous subsection) and a fine interpolated grid (right column; 0.5° x 0.05 km grid extending from 2 km to 50 km height). The rows show the three cases of "background" (top), "medium" (middle), and "volcanic" (bottom) aerosol load, respectively.

4.1.4 Modeling of Aerosol Effects on Propagating IR Waves

The so-far-existing capabilities of EGOPS for propagation modeling of SWIR waves were implemented during the FFG-ALR ACCURAID project (2006/2007). The physical processes incorporated in the SWIR forward modeling are described by *ACCURAID* (2007b), which is why this will not be replicated here. The innovation during EOPSCLIM concerning the propagation modeling was that the user can now select between the Simple Aerosol Model and the more sophisticated SAGE II-based Aerosol Model of EGOPS (subsection 4.1.3).

Figure 4.4, left column, shows transmissions for the ACCURATE CO_2 absorption (2095.724 nm) and reference (2096.300 nm) channel through aerosol laden air computed with EGOPS forward modeling. The right column shows the difference in transmissions comparing aerosol laden air with aerosol free (no aerosol load) air. The influence of background, medium and volcanic aerosol load are shown assuming a tropical occultation event (i.e., the FASCODE tropical atmosphere was used as background). As visible from Figs. 4.2 and 4.3, the aerosol extinction coefficient is largest over tropics, which is why these results reflect the "worst case" of the influence of aerosols. The forward modeling included the same atmospheric influences as used for the forward modeling transmission results shown in subsection 3.1 of *ACCURAID* (2007b). These are trace species extinction, Rayleigh scattering, scintillation fading and aerosol extinction. The only difference is that the SAGE II based aerosol model was used instead of the simple aerosol model used at that time.

As one can see, the attenuating influence of aerosols on the signal is very small in background and medium aerosol laden air. It reaches a maximum of 1 dB at height 5 km. The influence of volcanic aerosol load, however, is significant according to this new model, which is probably conservative, though, in the sense that the actual fall-off of extinction with increasing wavelength may be stronger at wavelengths > 1500 nm than estimated near 1000 nm as done here. The attenuation due to volcanic aerosol load is largest (up to 4 dB) in the lower stratosphere, where a huge amount of aerosols tends to be present after volcanic eruptions.

Favorably in the lower stratosphere the ACCURATE signal-to-noise ratio is very strong (see, e.g., also *ACCURAID*, 2007a) so that an additional damping of around 3 dB has fairly limited effect on retrieval performance. The upper troposphere is significantly influenced, too, where the attenuation induced by aerosols amounts to about 3 dB. Nevertheless, in every case the transmitted signal appears still adequately strong so as to ensuring the possibility to accurately derive atmospheric trace gas profiles even in air shadowed by aerosol immediately after a major volcanic eruption.

Figure 4.4 (right column with aerosol contribution isolated) also shows that due to the close vicinity of absorption and reference channel in the ACCURATE channel setup (*ACCURAID*, 2007a) the aerosol effect will very accurately cancel when building the differential transmission signals for subsequent retrieval of trace gas profiles or the line-of-sight wind profile.

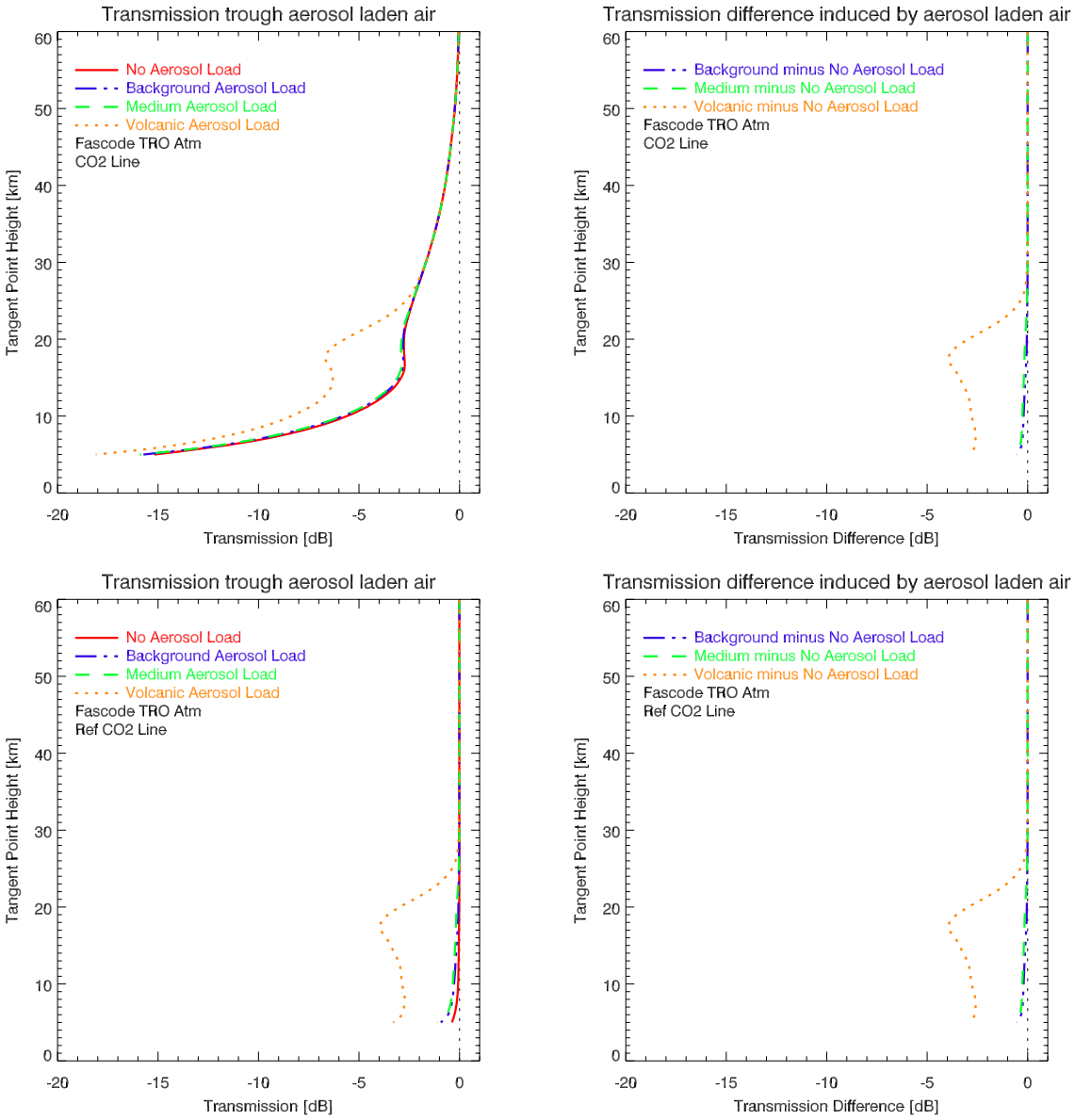

Figure 4.4: Propagation modeling results for the ACCURATE CO_2 absorption (upper row) and reference (lower row) channels in air with no (red, solid), background (blue, dashed-dotted), medium (green, dashed), and volcanic (orange, dotted) aerosol load, respectively. The left panels show direct transmission results and the right ones the difference between the transmissions of aerosol laden air vs. clear air.

4.2 Development of an Initial Wind Retrieval System

The second part of the EGOPS enhancements under EOPSCLIM concerning the LIO capabilities comprised the development of an initial wind retrieval system. The capabilities for modeling influence of wind on propagating SWIR signals were already implemented within the scope of the FFG-ALR ACCURAID project (cf. *ACCURAID*, 2007b). An initial assessment of the retrieval accuracy of wind velocity in line-of-sight (l.o.s) direction of an occultation event was performed, too, within the scope of ACCURAID (cf. *ACCURAID*, 2007a). But this was done using a simple error estimation tool external of EGOPS, the so-called ALPS (ACCURATE LIO Performance Simulator) which is fed by transmissions calculated using RFM (Reference Forward Model, *RFM* 1996, 2008).

Within the scope of EOPSCLIM, an initial chain for retrieving l.o.s wind velocity was implemented into EGOPS, which evaluates transmissions simulated using the forward modeling, observation system modeling and transmission retrieval parts of EGOPS. The following subsections give an overview on the retrieval chain (subsection 4.2.1) and show first simulation results (subsection 4.2.2).

4.2.1 Implementation of the Wind Retrieval from SWIR Signals

The initial retrieval of wind velocity in line-of-sight direction of an occultation event, shortly l.o.s. wind (V_{los}), is based on a double-difference of logarithmic transmissions (which are retrieved from observed/forward modeled signal amplitudes) of two so-called SWIR wind channels (Tr_{w1}, Tr_{w2}) and a suitable non-absorbing reference channel (Tr_{Ref}): $\Delta\Delta Tr_{\mathrm{w1w2}}$ [dB] = (Tr_{w1}-Tr_{Ref}) – (Tr_{w2}-Tr_{Ref}). The two wind channels are located at the two turning points of an arbitrary absorption line (cf., e.g., Fig. 6 from *ACCURAID*, 2007a). It is advantageous if the absorption line being used is symmetric, from a globally well-mixed weakly varying gas, and only weakly dependent on temperature and pressure conditions.

The ACCURATE CO_2 line is applicable for this purpose and presumably also the ACCURATE $C^{18}OO$ absorption line. Because of the symmetry of the used absorption line, the transmissions Tr_{w1} and Tr_{w2} differ (if ideally symmetric) from zero only in the case that wind is blowing and inducing a Doppler shift $\mathrm{d}\nu_{\mathrm{w}} = -(\nu_0/c_0)\cdot V_{\mathrm{los}}$, where c_0 is the speed of light and ν_0 is the frequency in the center of the absorption line in use. Further ingredients for the initial wind retrieval are the modeled transmission derivatives $(\mathrm{d}Tr/\mathrm{d}\nu)_{\mathrm{w1,Mod}}$ and $(\mathrm{d}Tr/\mathrm{d}\nu)_{\mathrm{w2,Mod}}$ at the two wind channels, which are computed using a propagation model and used as a priori information to quantify the change of transmission with frequency change (transmission sensitivity to wind-induced Doppler shift) at and in the vicinity of the wind channels. Furthermore, the difference of the modeled transmissions at the two wind channels, ($\Delta Tr_{\mathrm{w1w2,0,Mod}}$), is computed from the propagation model, which is only needed in order to compensate for potential asymmetries of the used absorption line.

Thus, the "wind retrieval equation" is as follows (after *ACCURAID*, 2007a):

$$V_{\mathrm{los}}\,[\mathrm{m/s}] = -\frac{c_0}{\nu_0}\cdot \mathrm{d}\nu_{\mathrm{w}} = -\frac{c_0}{\nu_0}\cdot\frac{\mathrm{d}Tr}{\mathrm{d}Tr/\mathrm{d}\nu} = -\frac{c_0}{\nu_0}\cdot\frac{(\Delta\Delta Tr_{\mathrm{w1w2}} - \Delta Tr_{\mathrm{w1w2,0,Mod}})}{(\mathrm{d}Tr/\mathrm{d}\nu)_{\mathrm{w1,Mod}} - (\mathrm{d}Tr/\mathrm{d}\nu)_{\mathrm{w2,Mod}}}\cdot \qquad (4.3)$$

Since the retrieval of transmissions needs knowledge of the atmospheric refractivity and since it is hard to accurately derive this refractivity from SWIR signals itself (because it is difficult to measure phase delays induced by atmospheric refractivity from short wavelengths) it is necessary to derive first atmospheric refractivity from LMO (LEO-LEO Microwave Occultation) data in order to be able to subsequently derive atmospheric parameters from SWIR signals (as a fall back, with reduced accuracy and degradation of un-biasedness of parameters, profiles from atmospheric analyses such as of ECMWF can be used).

Thus in a self-calibrated essentially model-independent observing system it is necessary to always use LIO in combination with LMO. The connection of the LMO and the LIO retrieval is shown in Figure 4.5 (with the LMO part in the figure called LRO from an earlier notation).

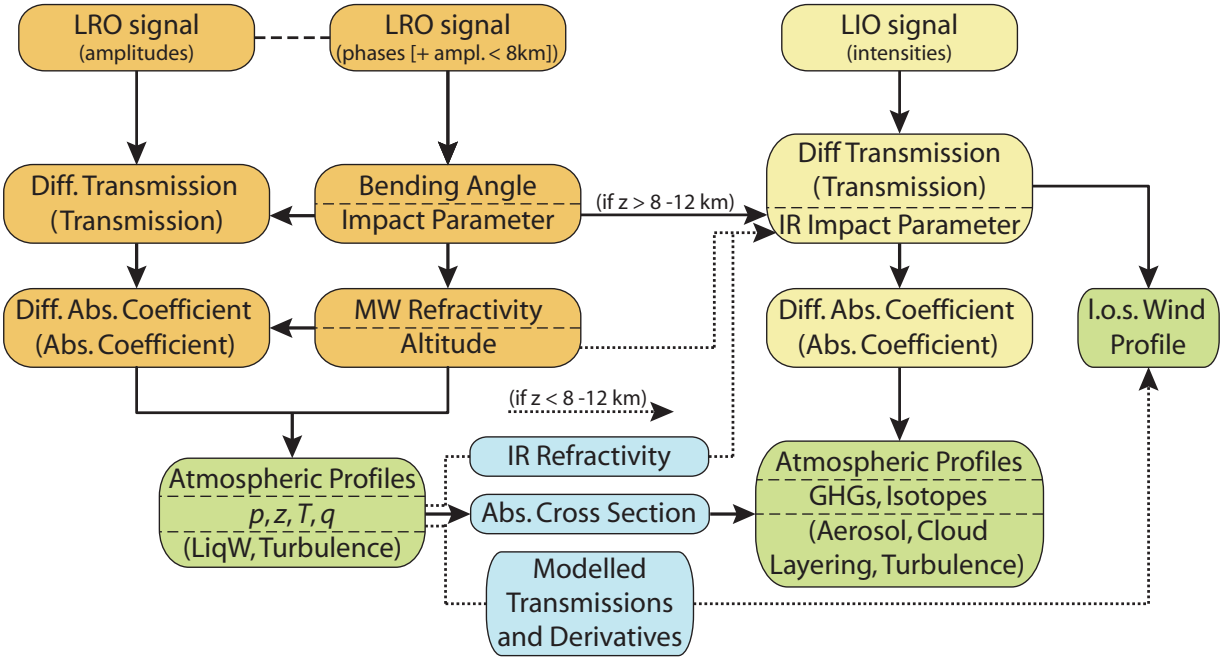

Figure 4.5: Overview on the LIO+LMO retrieval processing.

As seen from Figure 4.5, concerning the SWIR part, the wind retrieval needs the transmissions and corresponding impact heights (or impact parameters, which are the impact heights including the local radius of curvature) retrieved from the SWIR w1 and w2 channels as well as the modeled transmissions and their derivatives. The initial wind retrieval capability implemented into the EGOPS retrieval system consequently concentrated on furnishing the SWIR transmission retrieval, on furnishing access to modeled transmissions via implementation of respective capabilities of the RFM model, and on implementing the wind retrieval equation itself. The LMO retrieval capabilities are an already-existing feature of EGOPS which is why no actions have been undertaken on this side.

In line with Figure 4.5, the EGOPS l.o.s wind retrieval first computes the IR impact parameters a at each channel. In the case of wind retrieval, which is only performed above a height of 10 km (compliant with the LIO wind retrieval requirements; cf. Table 1 of *ACCURAID*, 2007a), the IR impact parameters closely resemble the impact parameters derived from MWO. Afterwards, the transmissions at the two wind channels and the reference channel

(which is propagated twice in order to be able to account for different signal noises since, in reality, the reference signal will also be measured twice) are computed from the amplitude A of the signals using a standard routine for the retrieval of transmissions contained in EGOPS,

$$Tr_j(a_i) = -20 \cdot (\log A_j - \log A_j^{\mathrm{dsm}}) \quad [\mathrm{dB}], \tag{4.4}$$

where A_j^{dsm} is a normalization amplitude, which also serves for correction of the influence of defocusing and spreading. The indices j and i indicate the number of channels and height levels, respectively.

A challenging part of the integration of the wind retrieval into EGOPS was the implementation of a capability for derivation of the modeled transmissions and their derivatives. The transmission model used for this purpose was the RFM model and the basis for the calculation of the modeled transmissions are pressure and temperature retrieved just before from the MWO channels. Within the scope of the ACCURAID project, RFM has already been implemented into EGOPS in order to enable the computation of molecular absorption coefficients within the SWIR range as part of the signal propagation in forward modeling. This capability was enhanced during EOPSCLIM so that it is now possible to compute SWIR transmissions, too, using RFM within the EGOPS environment. For this purpose, the patch linking RFM with the EGOPS software was extended. The reason why this task was especially challenging is that the code structure of the RFM software is not readily linked in a seamless manner.

The final part of the enhancements comprised the computation of the modeled transmission and their derivatives at the two wind channels (the latter by finite-difference estimation over a small frequency step about the wind channel center frequency) and the implementation of the wind retrieval equation (Eq. 4.3). Including this, EGOPS now contains a full initial wind retrieval chain which enables to derive l.o.s. wind velocity profiles at the tangent point of an occultation event with good accuracy at least in smooth wind conditions (see subsection 4.2.2).

In the future, this initial, local wind retrieval will be complemented by an advanced, non-local wind retrieval which will exploit the information gathered during the whole occultation paths via application of an appropriate Abel transform. This advanced retrieval is expected to deliver accurate wind velocities also in non-smooth wind conditions.

4.2.2 Initial Wind Retrieval Results

This subsection presents some l.o.s. wind velocity retrieval results produced by using the initial EGOPS wind retrieval system. In addition, transmission double-differences ($\Delta\Delta Tr_{\mathrm{w1w2}}$ [dB], "delta-differential transmission") derived from forward modeled as well as retrieved transmissions, respectively, are shown.

Delta-differential transmissions ($\Delta\Delta Tr_{\mathrm{w1w2}}$ [dB]) derived from transmissions computed via propagation modeling of EGOPS are presented in Figures 4.6 and 4.7. In particular, the behavior of the delta-differential transmission in various atmospheric conditions assuming different wind cases are shown (for details, see figure captions). Concerning atmospheric influences on the transmission, defocusing loss, trace species absorption, Rayleigh scattering loss,

scintillation fading and background aerosol loss effects (computed with the simple aerosol model) were accounted for during propagation modeling. Measurement errors were not included in the transmissions underlying these figures, but they were superimposed in a step between propagation modeling and retrieval (effects showing up in Figs. 4.8 and 4.9).
The transmission differences of Figures 4.6 and 4.7 were already shown in a very similar manner in Figs. 8 and 7 of *ACCURAID* (2007b). Since comparison to those figures verifies that the behavior of the double difference transmissions did not change since the ACCURAID project (despite many upgrades to the EGOPS system meanwhile) this verifies that the SWIR forward modeling part of EGOPS still works smoothly.

Figures 4.8 and 4.9 show the same as Figures 4.6 and 4.7 for the transmissions retrieved within the scope of the wind retrieval. Basis for this wind retrieval were the SWIR transmissions used in Figs. 4.6 and 4.7 but in addition processed through the observation system modeling and impaired there by modeled instrumental (receiver) noise in the same way as in *ACCURAID* (2007b) (cf. Fig. 10 therein).
In general, the retrieved delta-differential transmissions show the same behavior as the forward modeled delta-differential transmissions. In this way it is verified that the retrieval of SWIR transmissions works basically well. The jitter of the retrieved transmissions is due to the errors (receiver noise, in particular) superimposed on the forward modeled signal intensities in the observation system modeling before the transmission and wind retrieval started.

Finally, Figures 4.10 and 4.11 show the wind retrieval results for the same occultation events as shown in the preceding figures (for details see figure captions). In general, the behavior of the retrieved wind velocities resembles the behavior of the true wind velocities underlying the SWIR propagation modeling (Fig. 4.6., upper-left panel). Thus this initial wind retrieval is already a useful instrument for studying the performance of wind retrieved from LIO measurements. The retrieval works best if smooth wind conditions are prevailing, as exemplified by the case of constant wind velocity during the whole occultation event. If wind is, for example, changing from positive to negative values (which means that it alternately blows in l.o.s and against l.o.s direction with varying speed as exemplified by the sinusoidal wind case), the magnitude of the wind vector is significantly underestimated and the whole sinusoidal shape is moved downwards (that is the sinusoidal profile is damped and downward-phase-shifted in the retrieval). These limitations are intrinsic to the applied initial local-wind retrieval approach (Eq. 4.3), since with this ansatz the retrieved wind profile is locally linked to reflect the behavior (e.g., a downward phase shift) of the delta-differential transmission profile.

A future advanced non-local retrieval approach, exploiting information from the whole occultation paths via using an appropriate Abel transform (as shortly mentioned in the previous subsection), is expected to be essentially free from the effects mentioned above. This is why it is expected that such advanced wind retrieval will also in non-smooth wind conditions deliver results achieving the accuracy as estimated within ACCURAID using the ALPS error estimation tool (cf. Fig. 14 of *ACCURAID*, 2007a).
The development of this enhanced wind retrieval as well as a closer investigation of the characteristics and limitations of the initial local wind retrieval will be subject of future research.

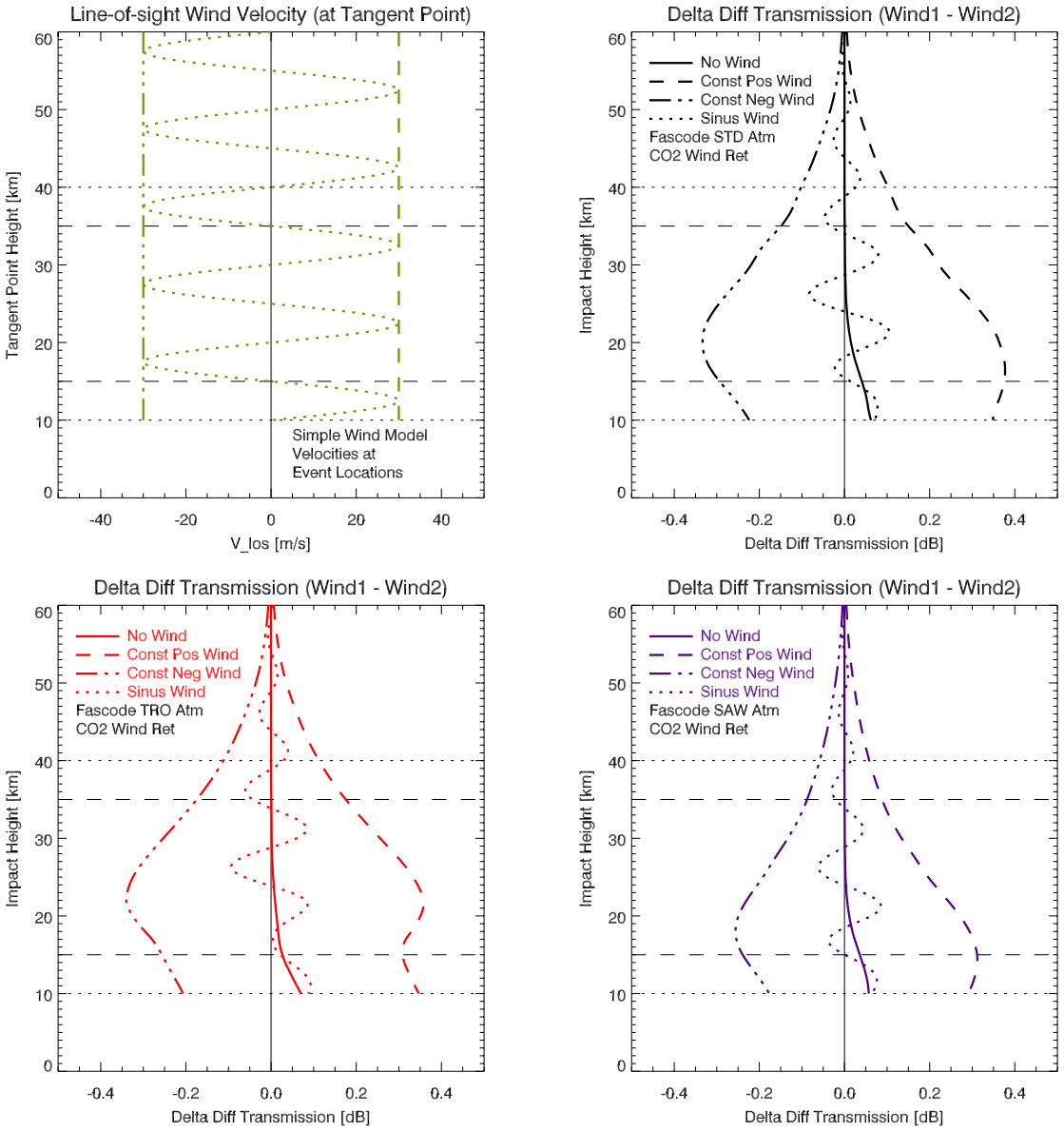

Figure 4.6: Delta-differential transmissions $\Delta\Delta Tr_{w1w2}$ [dB] derived from w1 and w2 transmissions around the ACCURATE CO_2 channel computed with the forward modeling part of EGOPS assuming four different wind conditions (shown in the upper left figure): constant positive wind (dashed), constant negative wind (dash-dotted), sinusoidally in height varying wind (dotted), and no wind (solid). The results are shown for three different atmospheric conditions using ideal geometry: FASCODE standard (STD, upper right), tropical (TRO, lower left) and sub-arctic winter (SAW, lower right) atmosphere. The horizontal lines indicate the ACCURATE target (dotted) and threshold (dashed) requirements set for the height range where l.o.s wind profiles shall be provided. The results are comparable with Fig. 8 of *ACCURAID* (2007b).

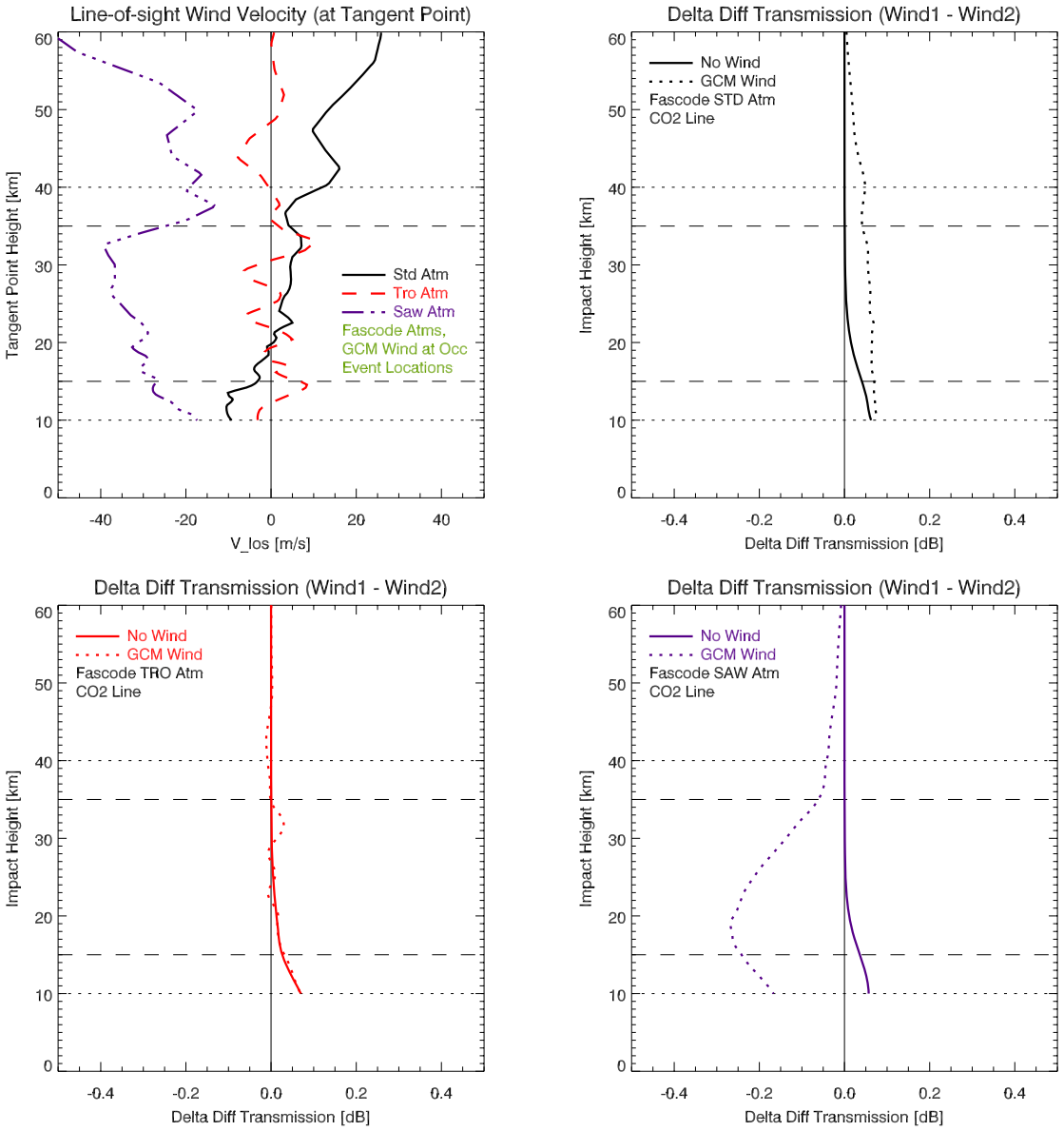

Figure 4.7: Delta-differential transmissions $\Delta\Delta Tr_{w1w2}$ [dB] derived from w1 and w2 transmissions around the ACCURATE CO_2 channel computed with the forward modeling part of EGOPS using real geometry and wind velocity at the tangent point taken from an ECMWF climatology of July 15, 2006. No wind (solid) and GCM wind (dotted) are shown. The results are shown for three different atmospheric conditions: FASCODE standard (STD, upper right), tropical (TRO, lower left) and sub-arctic winter (SAW, lower right) atmosphere. The horizontal lines indicate the ACCURATE target (dotted) and threshold (dashed) requirements set for the height range where l.o.s wind profiles shall be provided. The results are comparable with Fig. 7 of *ACCURAID* (2007b).

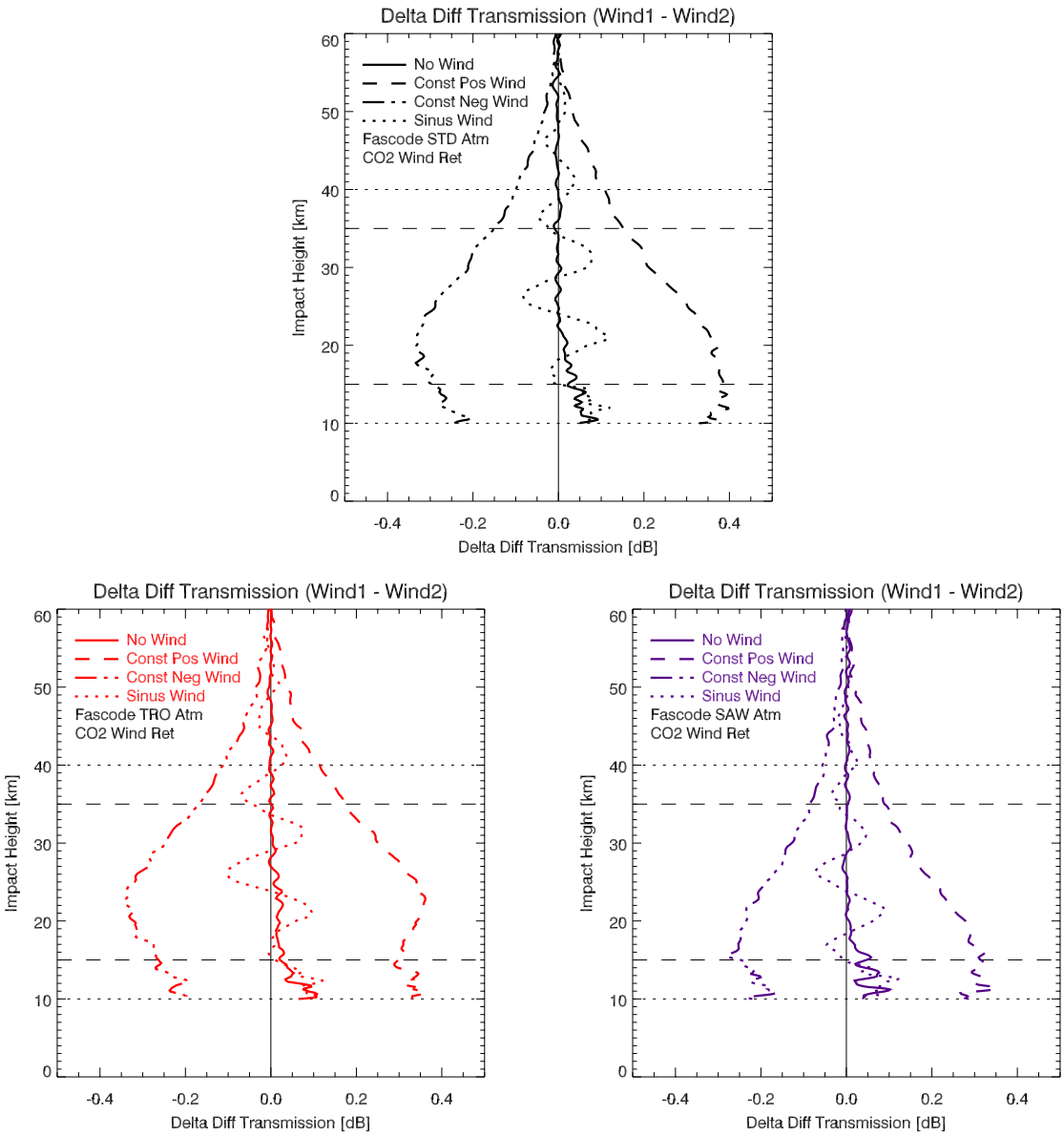

Figure 4.8: Same layout as Figure 4.6 (except the upper-left panel of that figure not repeated and the upper right shifted to center), but here the transmission retrieval results are shown.

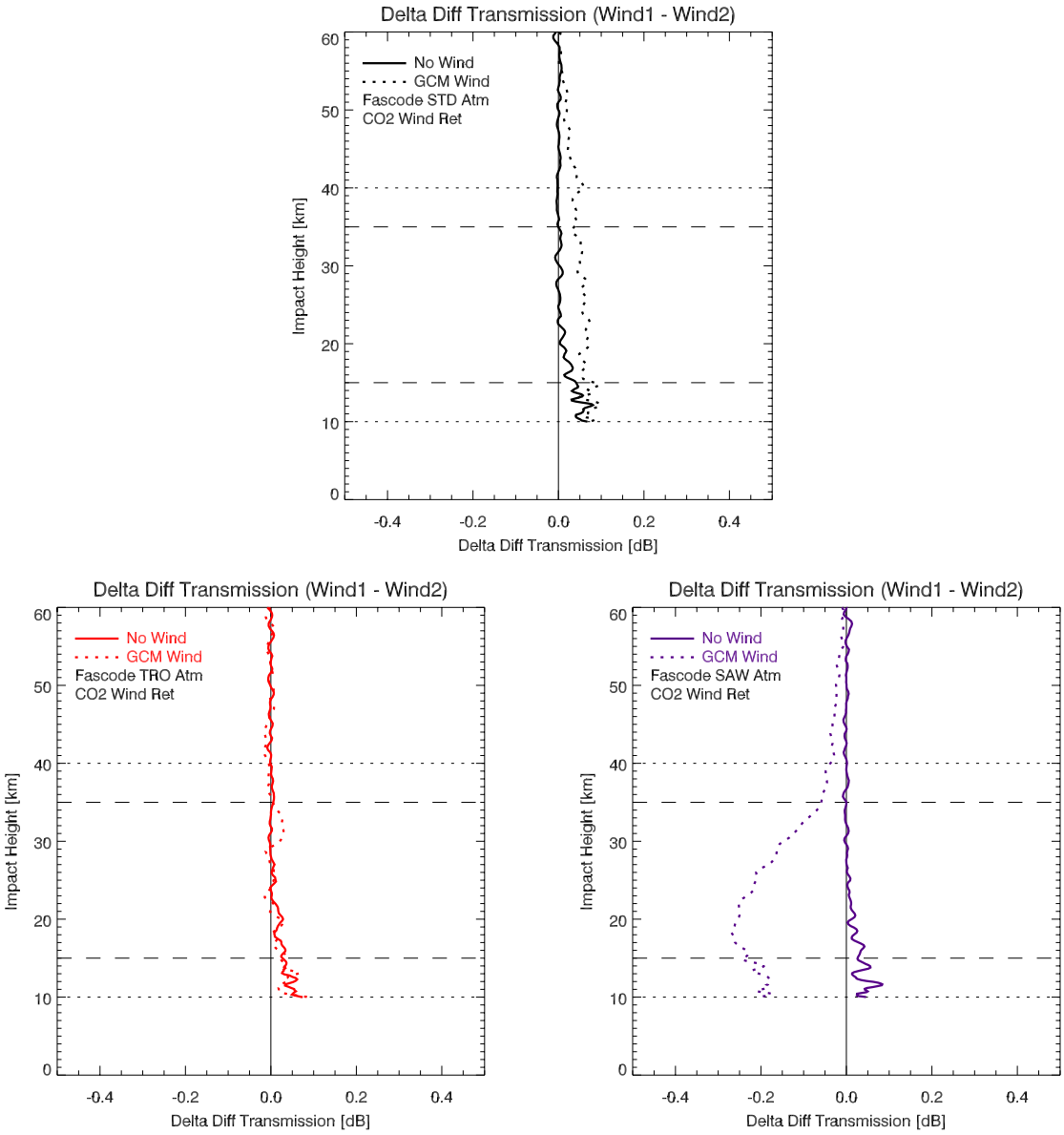

Figure 4.9: Same layout as Figure 4.7 (except the upper-left panel of that figure not repeated and the upper right shifted to center), but here the transmission retrieval results are shown.

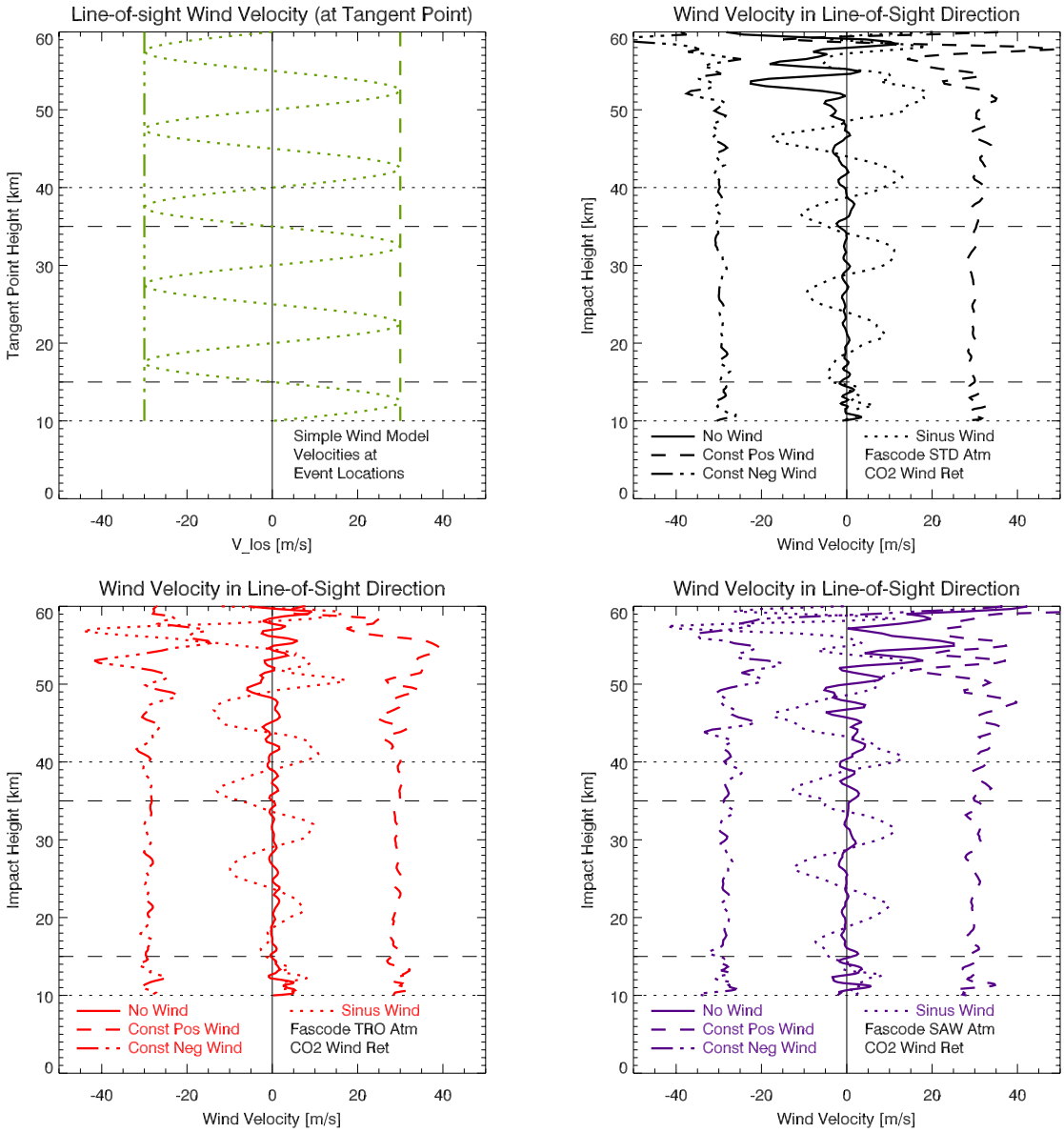

Figure 4.10: Initial wind retrieval results: retrieved wind velocities for the same occultation events and atmosphere and wind conditions as shown in Figure 4.6. The upper left panel shows the "true" wind velocities at occultation event location underlying the SWIR propagation modeling; the other three panels show the retrieval results.

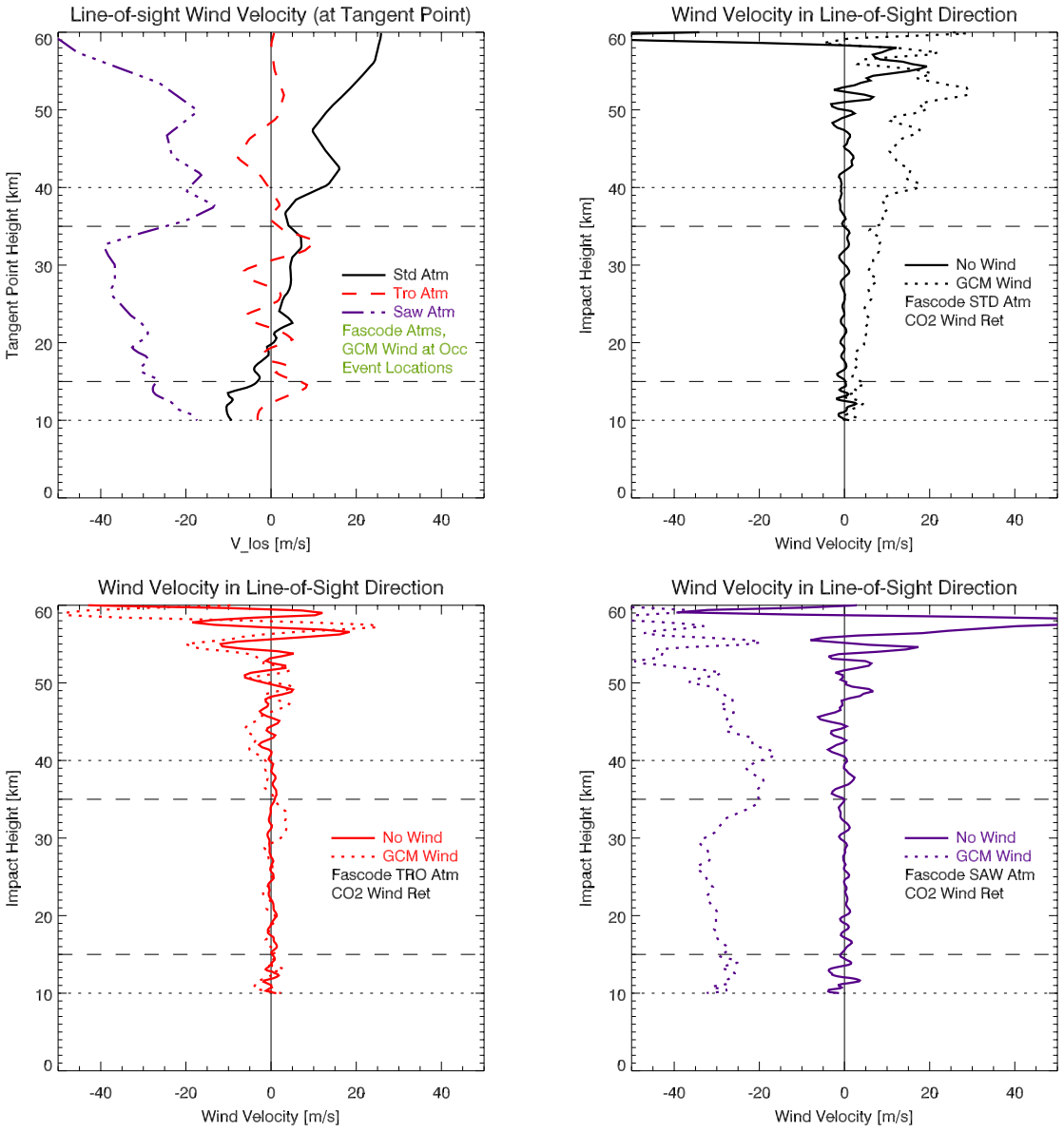

Figure 4.11: Initial wind retrieval results: retrieved wind velocities for the same occultation events and atmosphere and wind conditions as shown in Figure 4.7. The upper left panel shows the "true" wind velocities at occultation event location underlying the SWIR propagation modeling; the other three panels show the retrieval results.

5 Summary and Outlook

The EOPSCLIM project contributed to software enhancement of the WegCenter's end-to-end occultation simulator and processing system ("EGOPS") along two main lines: 1) contribution to the integration of real RO data processing within EGOPS, including on the new MetOp GRAS data stream, and 2) advancement of the new ACCURATE infrared laser occultation functionality within EGOPS by aerosol modeling and by a first version of wind profile retrieval processing.

This report described the results of this EGOPS software advancement work under the EOPSCLIM project both regarding the results of the work on real RO data processing and on the ACCURATE infrared laser occultation advancements, respectively.

In summary, the integration of real GPS RO data processing into EGOPS and the subsequent enhancements from CCRv2.3 status to OPSv5.4 were successful. The integration also greatly facilitated further planned enhancements, where in particular advancement towards climate-quality moist air retrieval in the troposphere (including humidity retrieval) from real GPS RO data is an essential next step.

The inclusion of the new latitude-height-frequency-dependent aerosol extinction coefficient model based on SAGE II data turned out to be very useful. It enabled seamless integration of modeling aerosol effects on SWIR ray tracing signal propagation, and the results under different aerosol loading conditions ("background", "medium", "volcanic") look reasonable. Also the inclusion of an initial wind retrieval capability was found useful and it could be demonstrated that this simplified approach already delivers quantitatively useful wind profiles in smooth wind conditions. The initial performance analysis also provided valuable pointers to next steps for improvement.

Looking to the immediate future, the enhancement of EGOPS for both real GPS RO data processing as well as LIO end-to-end simulation is scheduled to be continued within the on-going FWF-CLIMROCC project and the new ESA-ACTLIMB study (performance of active limb sounding; ESA/ESTEC study) starting by May 2008 as well as the new ESA-MMValRO study (multi-mission validation by RO; ESA/ESRIN study) starting mid 2008. In addition, the on-going ESA-Prodex project on EGOPS6 System Development (until mid 2009) will provide important continued support at EGOPS S/W system engineering level also to these future EGOPS enhancements.

It is one major aim of these follow-on projects to further advance the EGOPS OPS system so that both real GPS RO and simulated ACCURATE LIO measurements can be processed with further improved quality, e.g., in the latter case for studying trace gas and wind retrieval performances in detail.

Acknowledgments. MetOp GRAS data were provided by EUMETSAT under the ESA/EUMETSAT Research Announcement of Opportunity (RAO) Project GRASIVAL (ID 3057, PI G. Kirchengast). We especially thank A. von Engeln and C. Marquardt (EUMETSAT Darmstadt, Germany) for their valuable support. We also thank UCAR (Boulder, CO, USA) for the provision of Formosat-3/COSMIC radio occultation data, GFZ (Potsdam, Germany) for providing CHAMP radio occultation data, and ECMWF (Reading, UK) for access to their global operational analysis data. Some financial support was received from the Austrian Science Fund by U. Foelsche, B. Pirscher, and M. Borsche (FWF project CLIMROCC, P18837), and by J. Fritzer (ESA-Prodex project on EGOPS6 System Development). This work was funded by the FFG-ALR project EOPSCLIM (Contract No. ALR-OEWP-CO-414/07).

References

ACCURAID (2007a), Kirchengast, G., and S. Schweitzer, ACCURATE LEO-LEO Infrared Laser Occultation Initial Assessment: Requirements, Payload Characteristics, Scientific Performance Analysis, and Breadboarding Specifications, *Tech. Rep. for FFG-ALR No. 3/2007*, 56 pp, Wegener Center, Univ. of Graz, Graz, Austria.

ACCURAID (2007b), Schweitzer, S., G. Kirchengast, and F. Ladstädter, Enhancement of the end-to-end occultation simulation tool EGOPS for enabling quasi realistic simulations of LEO-LEO IR laser occultation measurements, *Tech. Rep. for FFG-ALR No. 1/2007*, Wegener Center, Univ. of Graz, Graz, Austria.

ACCURATE (2005), ACCURATE — Atmospheric Climate and Chemistry in the UTLS Region and climate Trends Explorer, *ESA Earth Explorer Core Mission Proposal/Ref.No. CCM2-13*, 19 pp, International Responding Team & WegCenter/UniGraz, Graz, Austria.

Borsche, M. (2008), Global Atmospheric Climatologies from Radio Occultation Data and Derivation of Diagnostic Parameters for Climate Monitoring, *Ph.D. thesis*, Wegener Center and Inst. for Geophysics, Astrophysics and Meteorology (IGAM)/Institute for Physics, University of Graz, Graz, Austria.

ECMWF (2006), ECMWF Newsletter – No. 110, *Tech. Rep*., ECMWF, Reading, UK, available at: http://www.ecmwf.int/publications/newsletters/chronological_list.html (August 2007).

Fjeldbo, G.F., V.R. Eshleman, and A.J. Kliore (1971), The neutral atmosphere of Venus as studied with the Mariner V radio occultation experiments, *Astron. J.*, 76, 123–140.

Foelsche, U., A. Gobiet, A. Loescher, G. Kirchengast, A.K. Steiner, J. Wickert, T. Schmidt (2005), The CHAMPCLIM Project: An overview, in: *Earth Observation with CHAMP: Results from Three Years in Orbit*, C. Reigber, H. Luehr, P. Schwintzer, J. Wickert (eds), Springer, Berlin Heidelberg, 615–619.

Foelsche, U., A. Gobiet, A.K. Steiner, G. Kirchengast, M. Borsche, T. Schmidt, and J. Wickert (2006), Global Climatologies Based on Radio Occultation Data: The CHAMPCLIM Project, in: *Atmosphere and Climate: Studies by Occultation Methods*, U. Foelsche, G. Kirchengast, A.K. Steiner (eds.), Springer, Berlin Heidelberg, 303–314.

Gobiet, A. (2005), Radio occultation data analysis for climate change monitoring and First climatologies from CHAMP, *Ph.D. thesis*, Wegener Center & IGAM/Institute for Physics, University of Graz, Graz, Austria.

Gobiet, A., and G. Kirchengast (2004), Advancements of GNSS Radio Occultation Retrieval in the Upper Stratosphere for Optimal Climate Monitoring Utility, *J. Geophys. Res.*, 109, D24110, doi: 10.1029/2004JD005117.

Gobiet, A., G. Kirchengast, L. Manney, M. Borsche, C. Retscher, and G. Stiller (2007), Retrieval of temperature profiles from CHAMP for climate monitoring: intercomparison with Envisat MIPAS and GOMOS and different atmospheric analyses, *Atmos. Chem. Phys*. *7* (13), 3519–3536.

GRAS-SAG (1998), The GRAS instrument on MetOp, ESA/EUMETSAT Rep. (ESA No. VR/3021/PI, EUMETSAT No. EPS/MIS/IN/9), ESA/ESTEC, Noordwijk, Netherlands.

Hajj, G.A., E.R. Kursinski, L.J. Romans, W.I. Bertinger, S.S. Leroy (2002), A technical description of atmospheric sounding by GPS occultation, *J. Atmos. Sol.-Terr. Phys.*, 64, 451-469.

Hajj, G.A., C.O. Ao, P.A. Iijima, D. Kuang, E.R. Kursinski, A.J. Mannuchi, T.K. Meehan, L.J. Romans, M. de al Torre Juarez, and T.P. Yunck (2004), CHAMP and SAC-C atmospheric occultation results and intercomparisons, *J. Geophys. Res.*, 109, D05109, doi: 10.1029/2003JD003909.

Healy, S.B (2001), Smoothing radio occultation bending angles above 40 km, *Ann. Geophys.*, 19, 459–468.

Healy, S. (2007), Operational assimilation of GPS radio occultation measurements at ECMWF, *Newsletter*, *111*, 6–12.

Healy, S.B., and J.R. Eyre (2000), Retrieving temperature, water vapour and surface pressure information from refractive index profiles derived by radio occultation: A simulation study, *Q. J. R. Meteorol. Soc.*, 126, 1661–1683.

Hedin, A.E (1991), Extension of the MSIS thermosphere model into the middle and lower atmosphere, *J. Geophys. Res.*, 96, 1159-1172.

Hocke, K., K. Igarashi, and T. Tsuda (2003), High-resolution profiling of layered structures in the lower stratosphere by GPS occultation, *Geophys. Res. Lett.*, 30, 8, 1426, doi: 10.1029/2002GL016566.

Kirchengast, G., J. Hafner, and W. Poetzi (1999), The CIRA86aQ_UoG model: An extension of the CIRA-86 monthly tables including humidity tables and Fortran95 global moist air climatology model, *Tech. Rep. for ESA/ESTEC No. 8/1999*, Inst. for Meteorol. and Geophys., Univ. of Graz, Graz, Austria.

Kirchengast, G., J.M. Fritzer, M. Schwaerz, S. Schweitzer, and L. Kornblueh (2004), The Atmosphere and Climate Explorer Mission ACE+: Scientific Algorithms and Performance Overview. *Tech. Rep. for ESA/ESTEC No. 2/2004*, IGAM, Univ. of Graz, Austria. [on-line: www.wegcenter.at/arsclisys > Publications]

Kirchengast, G., S. Schweitzer, J. Ramsauer, and J. Fritzer (2007), End-to-end Generic Occultation Performance Simulator version 5.2 (EGOPSv5.2) Software User Manual (Overview/ov, Reference/ref, and File Format/ff Manual), *Tech. Rep. for ESA/ESTEC No. 4/2007,* 62 pp (ov), 172 pp (ref), 97 pp (ff), Wegener Center & IGAM, Univ. of Graz, Graz, Austria, 2007 [on-line: www.wegcenter.at/arsclisys > Publications]

Kursinski, E.R., G.A. Hajj, J.T. Schofield, R.P. Linfield and K.R. Hardy (1997), Observing Earth's atmosphere with radio occultation measurements using the Global Positioning System, *J. Geophys. Res., 102,* 23,429–23,465.

Loiselet, M., N. Stricker, Y. Menard, and J.P. Luntama (2000), GRAS–Metop's GPS based atmospheric sounder, *ESA Bulletin 102*, 38-44, European Space Agency.

RFM (1996), High Level Algorithm Definition Document, *Rep. for ESA/ESTEC*, *Contract No.11886/96/NL/GS*, Institute of Atmospheric, Oceanic and Planetary Physics, Oxford University, United Kingdom.

RFM (2008), http://www-atm.physics.ox.ac.uk/RFM/, Internet, Mar. 2008.

Rieder, M.J., and G. Kirchengast (2001), Error analysis and characterization of atmospheric profiles retrieved from GNSS occultation data, *J. Geophys. Res.*, *106*, 31,755–31,770.

Rocken, C., R. Anthes, M. Exner, D. Hunt, S. Sokolovskiy, R. Ware, M. Gorbunov, W.S. Schreiner, D. Feng, B. Herman, Y.-H. Kuo, and X. Zou (1997), Verification of GPS/Met Data in the Neutral Atmosphere*, J. Geophys. Res*., *102* (D25), 29,849–29,866.

Rocken, C., Y.-H. Kuo, W.S. Schreiner, D. Hunt, S. Sokolovskiy, and C. McCormick (2000), COSMIC system description, *Terr. Atmos. Oceanic Sci*., *11* (1), 21–52.

Sokolovskiy, S. and D. Hunt (1996), Statistical optimization approach for GPS/Met data inversions, *Paper presented at URSI GPS/Met Workshop*, Tucson, Arizona.

SPARC (2008), http://www.sparc.sunysb.edu/html/RefData.html, Internet, Mar. 2008.

Steiner A.K., and G. Kirchengast (2005), Error analysis for GNSS radio occultation data based on ensembles of profiles from end-to-end simulations, *J. Geophys. Res.,* 110, D15307, doi: 10.1029/2004JD005251.

Syndergaard, S. (1998), Modeling the impact of Earth's oblateness on the retrieval of temperature and pressure profiles from limb sounding, *J. Atmos. Sol.-Terr. Phys.*, 60, 2, 171-180.

Syndergaard, S. (1999), Retrieval analysis and methodologies in atmospheric limb sounding using the GNSS radio occultation technique, *DMI Sci. Rep.*, 99-6, Danish Met. Inst., Copenhagen, Denmark.

Thomason, L., and Th. Peter (2006), Assessment of Stratospheric Aerosol Properties (ASAP), *SPARC* (Stratospheric Processes And their Role in Climate) *Report No. 4*.

von Engeln, A. (2006), A first test of climate monitoring with radio occultation instruments: Comparing two processing centers, *Geophys. Res. Lett.*, 33, L22705, doi: 10.1029/2006GL027767.

Vorob'ev, V.V., and T.G. Krasil'nikova (1994), Estimation of the accuracy of the atmospheric refractive index recovery from Doppler shift measurements at frequencies used in the NAVSTAR system, *Phys. Atmos. Ocean*, 29, 602-609.

Wang, D.-Y., G.P. Stiller, T. von Clarmann, et al. (2004), Cross-validation of MIPAS/ENVISAT and GPS-RO/CHAMP temperature profiles, *J. Geophys. Res.*, 109, D19311, doi: 10.1029/2004JD004963.

Wickert, J., C. Reigber, G. Beyerle, R. König, T. Marquardt, C. Schmidt, L. Grunwaldt, R. Galas, T. K. Meehan, W.G. Melbourne, and K. Hocke (2001), Atmosphere sounding by GPS radio occultation: First results from CHAMP, *Geophys. Res. Lett*., *28*, 3263–3266.

Wickert, J., T. Schmidt, G. Beyerle, R. König, C. Reigber, and N. Jakowski (2004), The radio occultation experiment aboard CHAMP: Operational data analysis and validation of vertical atmospheric profiles, *J. Meteor. Soc. Jap*., *82* (1B), 381–395, doi: 10.2151/jmsj.2004.381.

Wickert, J., G. Beyerle, R. König, S. Heise, L. Grunwaldt, G. Michalak, C. Reigber, and T. Schmidt (2005), GPS radio occultation with CHAMP and GRACE: A first look at a new and promising satellite configuration for global atmospheric sounding, *Ann. Geophys*., *23*, 653–658.

Wu, B.-H., V. Chu, P. Chen, T. King (2005), FORMOSAT-3/COSMIC science mission update, *GPS solutions 9*: 111–121, doi: 10.1007/s10291-005-0140-z.

– end of document –